Received: 1 April 2023 | Revised: 30 October 2023 | Accepted: 17 December 2023

DOI: 10.1002/qj.4645

Quarterly Journal of the Royal Meteorological Society RMetS

RESEARCH ARTICLE

Climate change quadruples flood-causing extreme monsoon rainfall events in Bangladesh and northeast India

Abdullah A. Fahad[1,2] | **Mahdi Hasan**[3] | **Noshin Sharmili**[4] | **Shammunul Islam**[5] | **Erik T. Swenson**[6] | **M. K. Roxy**[7]

[1]GMAO, NASA Goddard Space Flight Center, Greenbelt, Maryland, USA

[2]ESSIC, University of Maryland College Park, College Park, Maryland, USA

[3]Department of Marine, Earth and Atmospheric Science, North Carolina State University, Raleigh, North Carolina, USA

[4]Department of Geosciences, Pennsylvania State University, State College, Pennsylvania, USA

[5]Institute of Remote Sensing and GIS, Jahangirnagar University, Dhaka, Bangladesh

[6]Center for Ocean–Land–Atmosphere Studies, George Mason University, Fairfax, Virginia, USA

[7]Centre for Climate Change Research, Indian Institute of Tropical Meteorology, Pune, India

Correspondence
Abdullah A. Fahad, GMAO, NASA Goddard Space Flight Center, Greenbelt, MD, USA.
Email: a.fahad@nasa.gov

Funding information
Goddard Space Flight Center

Bangladesh and northeast India are the most densely populated regions in the world where severe floods as a result of extreme rainfall events kill hundreds of people and cause socio-economic losses regularly. Owing to local high topography, the moisture-carrying monsoon winds converge near southeast Bangladesh (SEB) and northeast Bangladesh and India (NEBI), which produces significant extreme rainfall events from May to October. Using observed data, we find an increasing trend of 1-day extreme event (>150 mm·day^{-1}) frequency during 1950–2021. The extreme rainfall events quadrupled over western Meghalaya (affecting NEBI) and coastal SEB during this period. Composite analysis indicates that warm Bay of Bengal sea-surface temperature intensifies the lower tropospheric moisture transport and flux through the low-level jet (LLJ) to inland, where mountain-forced moisture converges and precipitates as rainfall during extreme events. To understand the role of climate change, we use high-resolution downscaled models from Coupled Model Intercomparison Project phase 6 (CMIP6). We find that the monsoon extreme event increase is ongoing and the region of quadrupled events further extends over the NEBI and SEB in the future (2050–2079) compared with historical simulations (1950–1979). A quadrupling of the intense daily moisture transport episodes due to increased LLJ instability, a northward shift of LLJ, and increased moisture contribute to the increased future extreme events. This dynamic process causes moisture to be transported to the NEBI from the southern Bay of Bengal, and the local thermodynamic response to climate change contributes to the increased extreme rainfall events. The CMIP6 projection indicates that more devastating flood-causing extreme rainfall events will become more frequent in the future.

KEYWORDS

Bangladesh, climate change, CMIP, extreme rainfall, flood, India

1 | INTRODUCTION

The northeast region of Bangladesh (Sylhet division) and India (Meghalaya and Assam states) (NEBI) receives extremely high amounts of rainfall every year (>20 mm·day^{-1}, Figure 1) and is one of the wettest places on Earth (Murata et al., 2017). The mean rainfall in this region is primarily associated with the summer monsoon rainfall from June to September that contributes more than 70% of the total annual rainfall (Fahad et al., 2022). Owing to the exceptional mean rainfall of this region, extreme rainfall events are very frequent, causing flash floods and landslides in Bangladesh and northeastern India (Ahasan et al., 2010; Brouwer et al., 2007; Islam & Uyeda, 2007; Mahanta et al., 2013; Mishra et al., 2019; Shahid, 2011).

The NEBI region, especially the Meghalaya Plateau, experiences extreme rainfall that can lead to devastating flash floods in a short period of time (1–5 days) in the Sylhet and Sunamganj districts of Bangladesh (located in the south of Meghalaya Plateau) and the Assam state of India (located in the northeast of Meghalaya Plateau) (Figure 1a). Located in a lowland neighboring the Meghalaya Plateau, Sylhet and Sunamganj districts of Bangladesh experience heavy water flow from the Meghalaya foothills that can overflow local rivers (Brahmaputra and Surma rivers) and submerge more than 80% of the local regions under water. During 1981–2021, nearly 6.5 significant (>10 deaths) flash flood events per decade occurred due to extreme monsoon rainfall events over the Sylhet division of Bangladesh, and 4.5 events per decade over the Assam state of India (Figure 1b) (calculated based on International Disaster Database, http://www.emdat.be) (EMDAT, 2022). The Brahmaputra river and its tributaries, near the northwest of Meghalaya Plateau, can further carry the water to inland Bangladesh and flood regions near the river bank (e.g., Rangpur, Gaibandha, Kurigram, and Sirajganj), where monsoon-rainfall-related flood frequency is 3–4.5 per decade (Figure 1a,b). Southeast Bangladesh (SEB; Chittagong division) also experiences high flood frequency (~4.5 per decade) due to strong moisture convergences related to Arakan Mountain, and tropical-storm-related rainfall and storm surge owing to its location near the northern Bay of Bengal (BoB; Figure 1). As these regions frequently experience heavy rainfall in a short time-scale, landslide events are also frequent over hilly areas of Bangladesh (Sylhet and Chittagong) and northeast India (Meghalaya and Assam state) (Ahmed, 2015; Ahmed, 2021; Jamir et al., 2008; Mia et al., 2015; Phukon et al., 2012; Sarker & Rashid, 2013). During extreme rainfall events, fast-flowing water engulfing communities kills a significant number of people every year and dislocates most of the local communities from their homes. For instance, the July 2004 flood caused by heavy rainfall in the northeastern region affected nearly 50% of Bangladesh at its peak, as the Brahmaputra, Surma, and Meghna river basins overflowed, resulting in more than 600 fatalities and the displacement of 30 million people from their homes (EMDAT, 2022).

The mean summer monsoon rainfall over the NEBI and SEB regions is caused by the forced convergence of moisture by local mountains (Fahad et al., 2022). The warm sea-surface temperature (SST) over the BoB serves as a source of moisture during the summer monsoon that is transported by the low-level jet (LLJ) to the vicinity of the Arakan Mountains, Meghalaya Plateau, and Himalayan foothills. This further leads to the convergence of moisture and subsequent precipitation as rainfall (Fahad et al., 2022; Krishnamurthy & Shukla, 2000). As a result, three distinct rainfall maxima occur over the SEB (Chittagong), NEBI (Sylhet division of Bangladesh & Meghalaya Plateau of India), and northwest Bangladesh (NWB; Rangpur). Among these three maxima regions, the NEBI receives the largest mean monsoon rainfall and frequent extreme rainfall events (Rimi et al., 2019; Shahid, 2011; Tang et al., 2022) (Figure 1c,d).

The influence of tropical SST on the flooding events due to extreme rainfall events on the interannual time-scale over the NEBI is well known (Chowdhury & Ward, 2007; Rimi et al., 2019; Tang et al., 2022; Wahiduzzaman & Luo, 2021). SST anomalies related to the tropical Pacific (El Niño–Southern Oscillation, ENSO) and Indian Ocean (Indian Ocean Dipole, IOD) can influence the extreme rainfall events individually or all at once (Chowdhury & Ward, 2007) during the summer monsoon. However, the relationship between ENSO phases and seasonal flooding events in this region is not straightforward. Both the El Niño and La Niña phases of the ENSO can lead to increased seasonal mean extreme rainfall and flooding events (Chowdhury & Ward, 2007). The IOD also plays an important role as a low-frequency mode to increase the seasonal mean rainfall, though only over the western part of Bangladesh (Ahmed et al., 2017).

Owing to the increase in greenhouse gases in the atmosphere, the global water cycle significantly alters in a future climate (Douville et al., 2021). In a global warming scenario, the atmosphere warms and leads to increased moisture transport in the weather systems, which in turn increases seasonal mean precipitation and extreme events, especially over the tropical monsoon region (Doblas-Reyes et al., 2021; Douville et al., 2021). The annual mean extreme daily precipitation events increased over the past decades (1958–2018) and are projected to keep increasing over the north Indian monsoon region significantly (Seneviratne et al., 2021). Very few studies have analyzed the monsoon-related daily extreme

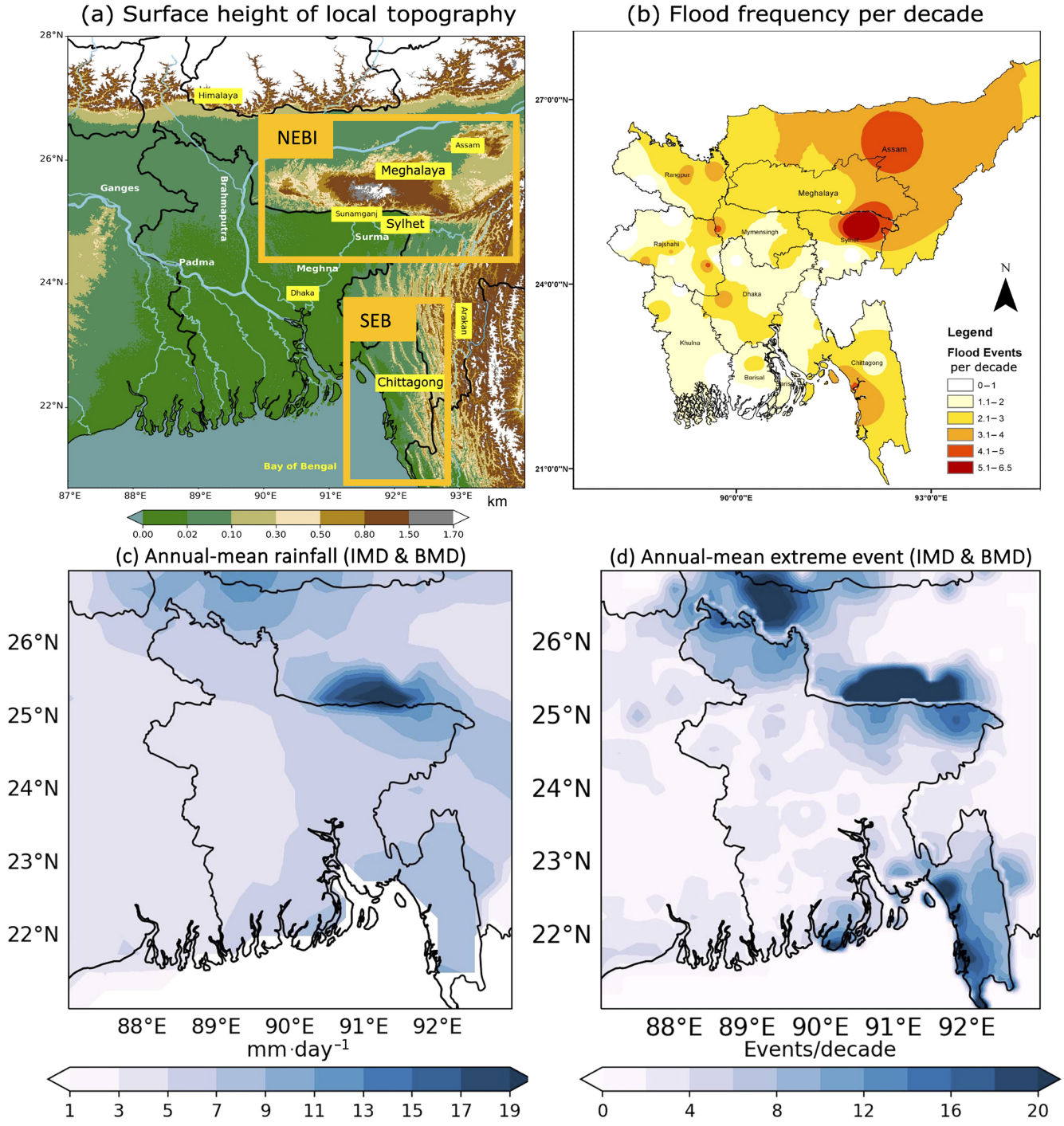

FIGURE 1 (a) Surface height of local topography (unit: km), and rivers of Bangladesh and northeastern India, (b) monsoon-rainfall-related flood frequency per decade, (c) observed annual mean rainfall (mm·day^{-1}), and (d) annual mean 1-day extreme rainfall event frequency per decade based on the India Meteorological Department (IMD) and Bangladesh Meteorological Department (BMD) gridded datasets from year 1981 to 2021. NEBI: northeast Bangladesh and India; SEB: southeast Bangladesh.

rainfall over Bangladesh and northeast India and explored the physical mechanisms behind it for the observed trends and future projections (Rimi et al., 2019; Shahid, 2011; Tang et al., 2022). Analyzing observed station data of Bangladesh, Shahid (2011) found that the heavy rainfall days over Bangladesh increased during the pre-monsoon season (April–May) from 1958 to 2007. The increasing trend in extreme rainfall events is consistent with the seasonal mean trend of rainfall, especially over NWB. However, Shahid (2011) could not draw a conclusion

on the influence of climate change on the observed trend. Focusing on the extreme rainfall in northeastern Bangladesh, Rimi et al. (2019) found 6 days of consecutive rainfall events with >150 mm accumulation doubles in the pre-monsoon season under a climate change scenario over northeast Bangladesh. Based on the HadRM3P model, Rimi et al. (2019) attributed that a flash flood in northeastern Bangladesh driven by an extreme rainfall event in March 2017 was most likely due to anthropogenic forcing, instead of internal variability modes such as IOD or ENSO. Later, Rimi et al. (2022) used a large ensemble regional climate model to investigate the influence of aerosols on the mean and extreme monsoon rainfall events, and found extreme rainfall events increase in the future due to global warming. The anthropogenic aerosols, however, suppress the increase of mean rainfall events during pre-monsoon and monsoon, whereas the increase of global mean surface temperature increases the rainfall (Rimi et al., 2022). Tang et al. (2022) analyzed the seasonal mean summer 2020 rainfall event over the northeast Indian subcontinent and found an anomalous anticyclone associated with the La Niña phase that contributed to the wettest summer rainfall event over this region since 1901. Tang et al. (2022) concluded that this type of extreme seasonal mean summer monsoon rainfall will likely increase in the future due to an increased water vapor transport under climate change.

The occurrence of flood events in the Sylhet division of Bangladesh, where flash floods are most frequent, is significantly dependent on extreme rainfall over the Meghalaya Plateau of India (Figure 1). However, most of the previous studies have only focused on the local station rainfall of Sylhet. We demonstrate that it is crucial to discuss rainfall behavior over northeast Bangladesh and India, including rainfall over Meghalaya, in the same context. Some major questions remain uninvestigated in previous studies, such as what drives the extreme events climatology of this region? How do flash-flood-causing extreme rainfall events and associated large-scale circulations evolve in a short time-scale? What drives the large trend in the observed and reanalysis of extreme events? What is the contribution of climate change? Do changes in the moisture content or associated wind circulation play a more important role in driving extreme events to change under global warming?

The aim of this study is to understand what drives the climatology and long-term trends of flood-causing extreme rainfall events over Bangladesh and northeast India, using observed stations and reanalysis data from approximately 1950 to 2021. We further explore the role of climate change in the change of extreme rainfall events, using high-resolution downscaled coupled climate models from the Coupled Model Intercomparison Project (CMIP) phase 6 (CMIP6), and comparing historical (1950–1979) simulations with SSP5-85 future projections (2050–2079) (extreme future scenario; Hausfather and Peters (2020)). To understand the contribution of moisture versus circulation change on extreme rainfall events, we investigate changes in thermodynamic and dynamic variables in a warming climate.

2 | METHODOLOGY AND DATA

The definition of extreme rainfall events can vary depending on the research question (Rimi et al., 2019; Roxy et al., 2017; Shahid, 2011; Tang et al., 2022). For a rainfall time series of station data without spatial dimensions, the 99th percentile or a value greater than two standard deviations is a good measure to define extreme rainfall events (Roxy et al., 2017). However, the percentile or standard deviation varies over spatial dimensions. For example, northeast Bangladesh receives maximum rainfall in this region with high variability, whereas western Bangladesh is relatively drier with low rainfall variability across time. Therefore, if we define extreme events with a percentile value and compare the spatial distribution of extreme events it will lead to unfair comparisons among different hydrological regions in the context of floods. To avoid this confusion, we defined a 1-day extreme rainfall event when the daily rainfall exceeds 150 mm (Rimi et al., 2019; Roxy et al., 2017). The rainfall days are counted if at least 0.1 mm of rainfall occurs in a day (Burls et al., 2019). The baseline climatology of extreme rainfall events can shift dramatically if a large trend is present in the time series (Thomas et al., 2023). To understand how the climatology of extreme rainfall events changes over the whole observed time series period used in this study, we calculated the ratio shown in Figure 2 as

$$\text{Ratio} = \frac{\text{Climatology}_{30} + \text{Change}_{\text{whole period}}}{\text{Climatology}_{30}}, \qquad (1)$$

where Climatology_{30} is the first 30 years of mean climatology of the number of events used as a baseline to compare and $\text{Change}_{\text{whole period}}$ is the 72-year trend of extreme rainfall events.

For the observed rainfall analysis, we used Bangladesh Meteorological Department (BMD) station data (https://www.bmddataportal.com) for Bangladesh from 1956 to 2021 and the India Meteorological Department (IMD) station data (https://cdsp.imdpune.gov.in) for India from 1950 to 2021. Gridded data analysis was done using the Enhancing National Climate Services (ENACTS)-BMD rainfall data over Bangladesh and IMD gridded data estimated from local station data from 1981 to 2021. The

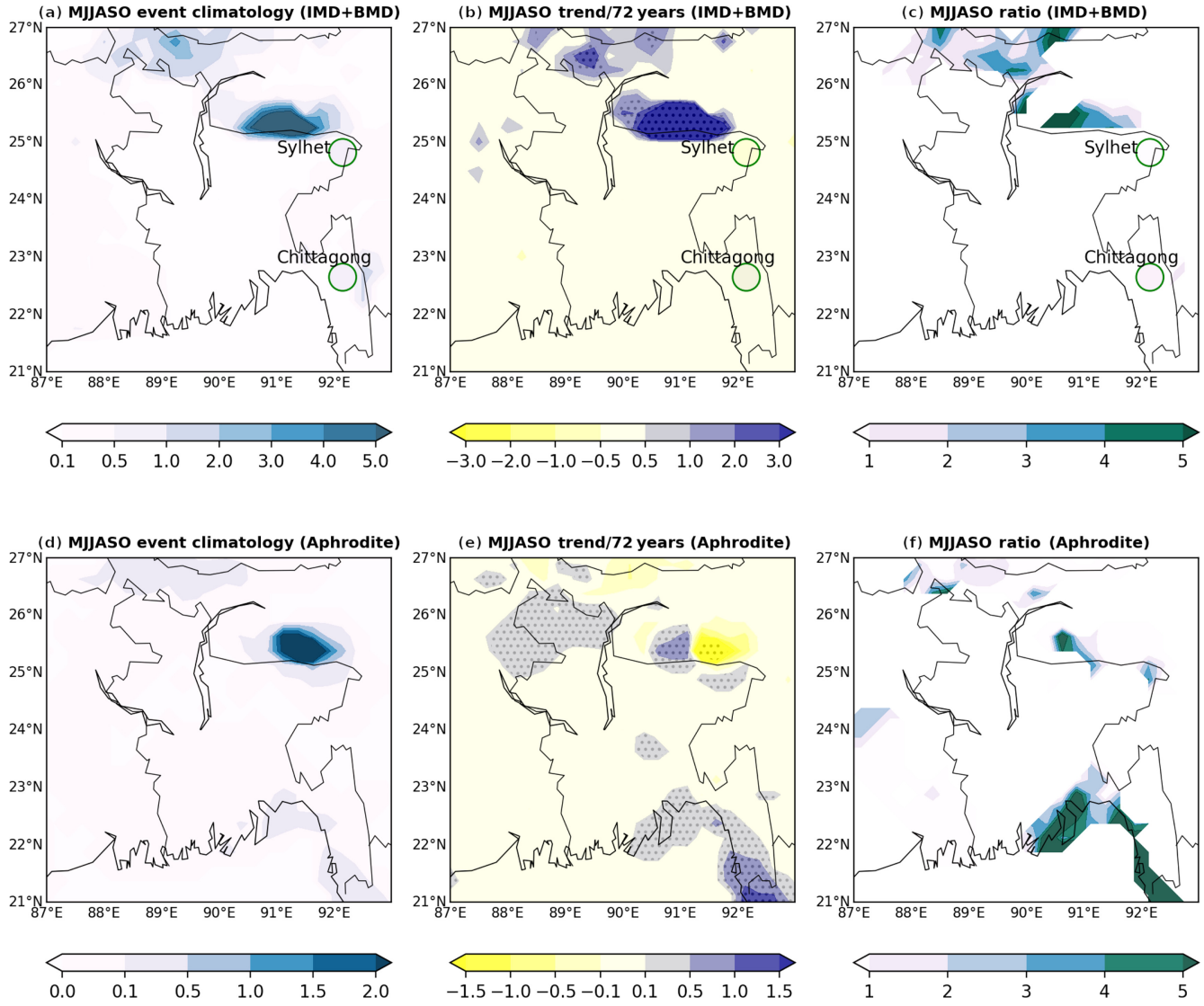

FIGURE 2 Based on years 1950–2021 India Meteorological Department (IMD) and Bangladesh Meteorological Department (BMD) (single station, circled over Sylhet and Chittagong that covers 1955–2021) data, plots show the May–October (MJJASO) (a) 1-day event climatology, (b) trends/72 years, and (c) ratio calculated based on Equation (1). Based on years 1951–2015 Asian Precipitation–Highly Resolved Observational Data Integration Towards Evaluation of Water Resources (APHRODITE) observed data, plots show the MJJASO (d) 1-day event climatology, (e) trends/72 years, and (f) ratio calculated based on Equation (1). Only significant trends and ratio at 95% confidence are shown in the (b), (c), (e), and (f).

ENACTS-BMD data are produced by merging station data from the BMD with satellite data that has a spatial resolution of 0.05∘ × 0.05∘ (Acharya et al., 2020). We calculated the flood frequency that had a significant impact (at least 10 human deaths) associated with monsoon rainfall using the International Disaster Database (http://www.emdat.be), which was interpolated to gridded data as shown in Figure 1b). For the observed surface height figure we used Global Multi-resolution Terrain Elevation Data (Danielson & Gesch, 2011). For the composite mean analysis of atmospheric circulation and ocean states from 1981 to 2021 we used the Modern-Era Retrospective Analysis for Research and Applications, Version 2 (MERRA-2) (Gelaro et al., 2017). For the longer period (1950–2021), we used National Centers for Environmental Prediction (NCEP)–National Center for Atmospheric Research (NCAR) Reanalysis (Kalnay et al., 1996) only for Figure 5a–c. The European Centre for Medium-Range Weather Forecasts Reanalysis v5 (ERA-5) (Hersbach, 2020) was also used over the period of 1950–2021 to diagnose dynamic versus thermodynamics drivers. For the observed BoB tropical cyclone and depression frequency, we used the International Best Track Archive for Climate Stewardship data (Knapp et al., 2010). We have also analyzed NASA's Integrated Multi-satellite Retrievals for Global Precipitation

TABLE 1 Coupled Model Intercomparison Project phase 6 high-resolution downscaled (0.25∘ × 0.25∘) model list.

Model name	Institution	Model name	Institution
1 ACCESS-ESM1-5	CSIRO	7 GFDL-CM4	NOAA-GFDL
2 CESM2	NCAR	8 INM-CM5-0	INM
3 CMCC-CM2-SR5	CMCC	9 IPSL-CM6A-LR	IPSL
4 CNRM-CM6-1	CNRM–CERFACS	10 MIROC-ES2L	MIROC
5 CanESM5	CCCma	11 MPI-ESM1-2-LR	Max Planck Institute
6 FGOALS-g3	CAS	12 NorESM2-MM	Norwegian Climate Center

Abbreviations: CAS, Chinese Academy of Sciences; CCCma, Canadian Centre for Climate Modelling and Analysis; CMCC, Euro-Mediterranean Centre on Climate Change; CNRM–CERFACS, Centre National de Recherches Météorologiques–Centre Européen de Recherche et de Formation Avancée en Calcul Scientifique; CSIRO, Commonwealth Scientific and Industrial Research Organisation; INM, Institute for Numerical Mathematics; IPSL, Institut Pierre-Simon Laplace; MIROC, Model for Interdisciplinary Research on Climate; NCAR, National Center for Atmospheric Research; NOAA-GFDL, National Oceanic and Atmospheric Administration Geophysical Fluid Dynamics Laboratory.

Measurement data for the 2022 precipitation analysis (Huffman et al., 2015). For observed data analysis we have also used Asian Precipitation–Highly Resolved Observational Data Integration Towards Evaluation of Water Resources (APHRODITE) data with 0.25∘ × 0.25∘ horizontal resolution from 1951 to 2015 (Yatagai et al., 2012).

To understand the impact of climate change on extreme rainfall events we used the latest generation of CMIP6 models (Eyring et al., 2016). However, the resolution of CMIP6 models is generally not high enough to study the impact of climate change on a regional scale such as Bangladesh and northeast India (Fahad et al., 2022). Fahad et al. (2022) found, 0.25∘ × 0.25∘ latitude–longitude spatial resolution or a higher is needed to resolve the rainfall variability over Bangladesh and northeast India owing to its unique topography. For this study, we used the latest version of the NASA Earth Exchange Global Daily Downscaled Projections (NEX-GDDP-CMIP6) (Thrasher et al., 2022) data that are available at the NASA Center for Climate Simulation data server (Schnase et al., 2011). The downscaled data are estimated from CMIP6 model outputs using a daily variant of the monthly bias correction/spatial disaggregation method (Thrasher et al., 2022). For this study, we used 12 CMIP6 downscaled models data that are in 0.25∘ × 0.25∘ spatial resolution and compared 30 years of historical simulation (years 1950–1979) with 30 years of future projection SSP5-85 (years 2050–2079) (Table 1). The CMIP6 downscaled multi-model mean (MMM) precipitation produces a reasonable spatial pattern and magnitude over the NEBI and SEB (Supporting Information Figure S2). A 68% intermodel consistency is equivalent to 95% statistical significance of a Student *t*-test, assuming models are independent of each other (Fahad et al., 2020; Power et al., 2012). As we have 12 model samples, we used stippling at a 90% significance level in figures to make the critical value more strict.

The vertically integrated moisture transport (VIMT) is calculated as (Fahad et al., 2022; Roxy et al., 2017):

$$\mathrm{VIMT} = \frac{1}{g}\left(\int_{p_{1,000}}^{p_{700}} qV\, dp\right). \tag{2}$$

The vertically integrated moisture flux convergence (VIMF) is calculated as (Fahad et al., 2022; Roxy et al., 2017):

$$\mathrm{VIMF} = \int_{p_{1,000}}^{p_{700}} \left(\frac{\partial uq}{dx} + \frac{\partial vq}{dy}\right) dp. \tag{3}$$

We used the algorithm developed by Thomas et al. (2020) to generate flood maps from Sentinel-1 (Agency, 2020) using Google Earth Engine.

3 | RESULTS

3.1 | Observed events and physical mechanism

The climatology of the annual mean 1-day (>150 mm/1 day) extreme rainfall events shows three regions with maxima: SEB, NEBI, and NWB (Figure 1d). In particular, the Meghalaya Plateau of the NEBI region experiences the largest 1-day rainfall events (>30 events per decade), which is consistent with the spatial pattern of the annual mean rainfall (Figure 1c). This is also consistent with the spatial pattern of the flood frequency (Figure 1b,d). Extreme rainfall events over the Meghalaya Plateau generate significant surface water that flows down to the relatively lower surface regions of the Sylhet division (especially Sylhet and Sunamganj districts) and Assam state, submerging low-lying areas very quickly and causing flash

floods (Figure 1a,b,d). Extreme rainfall events primarily occur from May to October (MJJASO) and are associated with the summer monsoon rainfall (Figures 2a,d and 1d). For our analysis and conclusions, we predominantly focus on the MJJASO season in this article. Figure 2b reveals a significant positive trend in 1-day rainfall events over the Meghalaya Plateau (part of NEBI) from 1950 to 2021, based on the IMD data during the MJJASO period. The Sylhet (part of NEBI) and Chittagong (part of SEB) stations, according to BMD data, exhibit a non-significant trend for extreme events. The 72-year linear trend from IMD data (1950–2021), when compared with the first 30 years' baseline (1950–1979), indicates that the frequency of summer monsoon extreme events has quadrupled during MJJASO (Figure 2c) over western Meghalaya, as calculated using Equation (1). To further validate results from the IMD dataset, we analyzed the APHRODITE observed gridded data (note that APHRODITE data covers only the years from 1951 to 2015). APHRODITE demonstrates a similar pattern with quadrupled extreme events over western Meghalaya that further extend over northern Bangladesh from 1951 to 2015 (Figure 2f). It is noteworthy that the MJJASO climatology for 1-day extreme rainfall events is weaker in APHRODITE than in IMD and BMD station rainfall data. For instance, the climatological mean over Meghalaya is approximately two events per MJJASO season in APHRODITE, whereas IMD indicates more than five events (Figure 2a,d). This discrepancy arises because APHRODITE data are processed as a relatively low-resolution gridded dataset compared with IMD and BMD and are limited in their temporal range.

The ratio calculated using the trend of APHRODITE extreme events over 72 years (the per-year trend multiplied by 72 years for comparison with the IMD data trend) indicates an increase in extreme events over western Meghalaya, similar to the IMD findings (Figure 2c,f). However, it shows a decreasing trend on the eastern side of Meghalaya. APHRODITE trend data indicate a shift in extreme rainfall events from eastern to western Meghalaya, contributing to the increased number of 1-day extreme rainfall events (Figure 2d,e). Figure 2e further displays an increasing extreme event trend over Sylhet (northeast Bangladesh), which extends from the Meghalaya region, and also suggests an increase in extreme events over Chittagong (SEB). The 72-year linear trend, in comparison with the first 30-year baseline (1950–1979), reveals that the frequency of summer monsoon extreme events—calculated using Equation (1)—based on the APHRODITE and IMD data reflects very similar changes. The extreme events during MJJASO have quadrupled over the past 72 years in western Meghalaya (Figure 2c,f). This increase in extreme events further extends to the Sylhet region in this time period (Figure 2f). Figures 2f and 3b further show a quadrupled or greater increase in extreme events over the SEB, particularly near Chittagong's coastal region. To further validate our findings, we investigate the ERA-5 data to compare the MJJASO seasonal trend and the ratio of extreme events and found a similar quadrupled increase in extreme precipitation events over the past 72 years (1950–2021) across NEBI and SEB (Supporting Information Figure S1).

Owing to discrepancies between the IMD station data and the APHRODITE gridded data, particularly in eastern Meghalaya, we used widespread extreme events to further analyze the physical mechanisms of extreme events (Figure 3a). We defined a widespread extreme event as when 150 mm of rainfall covers an area greater than 200 km^2 in a day in the Meghalaya region (longitude 90° E–92° E, latitude 25° N–26° N). Using widespread events should reduce the uncertainties that might arise due to using data from a single station. Over the years, the MJJASO widespread extreme event in Meghalaya has quadrupled, with noticeable year-to-year changes (Figure 3a, blue line). This change aligns with the average MJJASO seasonal rainfall in the Meghalaya area. For example, the seasonal average rainfall from 1950 to 1970 was lower than the rest of the record, leading to fewer extreme events during that time (Figure 3a). Figure 3c shows that the flood rate in Sylhet has also nearly quadrupled (0.985 per 72 years, 3.9 times compared with the 1960–1990 baseline). This is consistent with the increased rainfall and more frequent extreme events in western Meghalaya and Sylhet (Figure 3a). There is also an upward trend in flood frequency in the Chittagong division (SEB) consistent with the increased extreme rainfall events (Figures 2f and 3b,c). However, flood frequency in Assam (north of the Meghalaya Plateau) does not show a clear trend during the study period, indicating increased Meghalaya extreme rainfall events mostly affecting northern Bangladesh (Sylhet).

The seasonal mean summer monsoon rainfall over Bangladesh and northeastern India occurs due to the LLJ carrying moisture from the BoB to the north inland, where lower tropospheric moisture flux converges due to local mountains (Arakan Mountains, Meghalaya Plateau, and Himalaya foothills) that generates rainfall (Fahad et al., 2022). To understand the physical mechanism of extreme rainfall events in northeastern Bangladesh and India, we analyzed composite mean moisture transport and flux based on 188 widespread extreme events (1-day events) in the NEBI region (from 1981 to 2021). Figure 4 shows the composite mean of vertically integrated lower tropospheric (1,000–700 hPa) moisture transport (VIMT), and moisture flux (VIMF), V (wind speed), and Q (specific humidity) for the onset day (0-day lead) of the 1-day extreme rainfall events and their evolution.

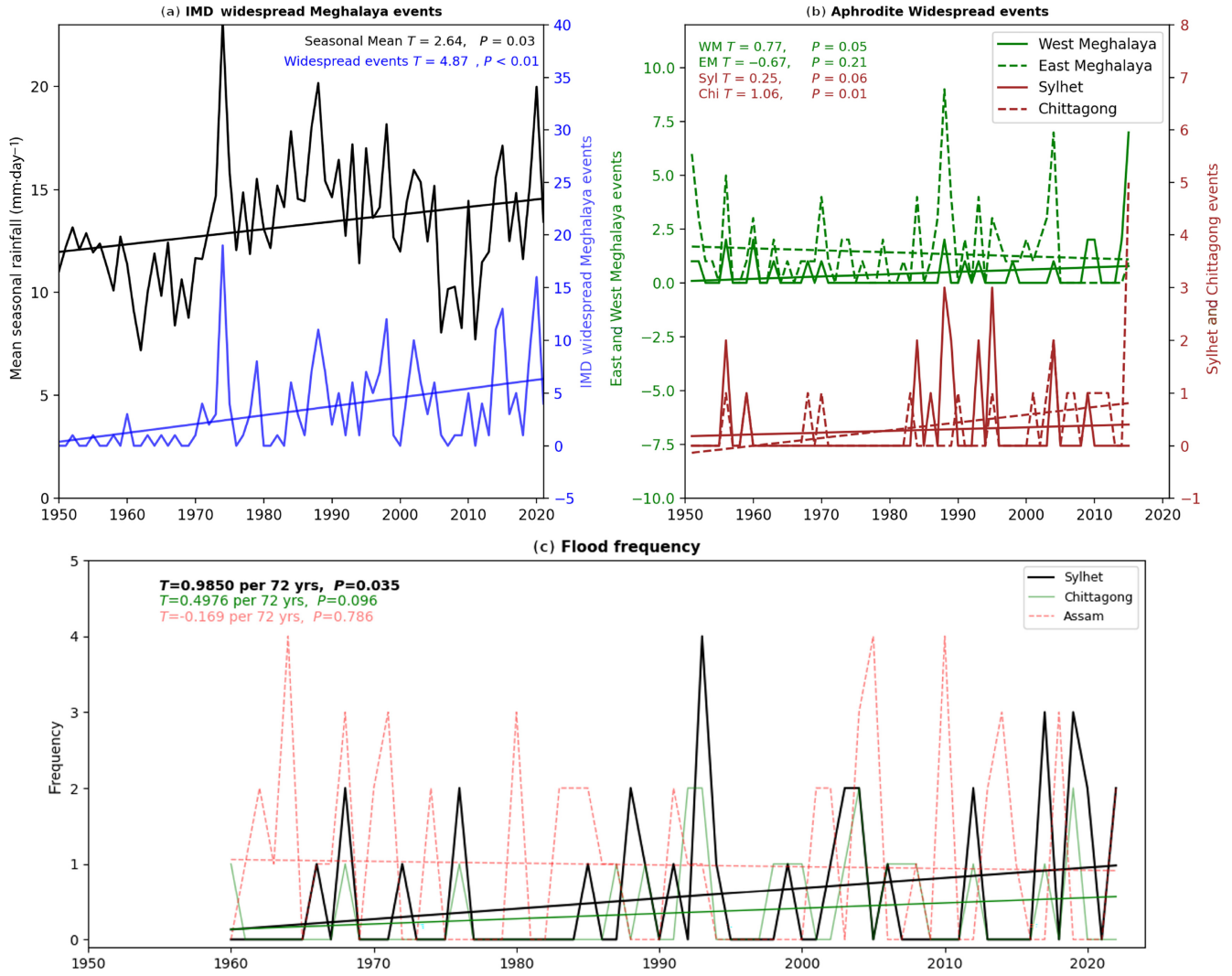

FIGURE 3 (a) Based on India Meteorological Department (IMD) data, widespread 1-day events over Meghalaya (black line), western Meghalaya (blue solid line), and eastern Meghalaya (blue dotted line). (b) Based on Asian Precipitation–Highly Resolved Observational Data Integration Towards Evaluation of Water Resources (APHRODITE) data, widespread 1-day events over the western Meghalaya (green solid line), and eastern Meghalaya (green dotted line), Sylhet (solid red line), and Chittagong (dotted red line). (c) The flood frequency per year. The time series for Sylhet, Chittagong, and Assam (northwest of Meghalaya) are presented in consistent black, blue, green, and red colors.

The composite mean of VIMT and VIMF shows that, during the onset day (0-day lead), the lower tropospheric moisture transport and convergence are significantly stronger over the NEBI, starting from the northern BoB, which leads to intense rainfall events (Figure 4a,b). The VIMT is maximum over the southeastern BoB during the 0-day lead, where VIMF divergence is also stronger (Figure 4a,b). The composite mean difference between the 9-days lead and 0-day lead and the 18-days lead and 0-day lead shows the evolution of VIMT and VIMF before the extreme rainfall events (Figure 4e,f,i,j). The lower tropospheric moisture transport and flux convergence both intensify from the northern BoB to the NEBI as extreme events occur during the 0-day, compared with the 9-days and 18-days lead. The divergence and moisture transport over the southern BoB, where LLJ is climatologically strongest during this season, also increase significantly during the onset of extreme events compared with the 9-days and 18-days lead, indicating potential moisture transport over the NEBI associated with the 1-day extreme events (Figure 4f,j). The VIMT and VIMF are at their maximum over the southern BoB during the 18-day and 9-day leads respectively. However, the maxima shift to the NEBI on the onset day (0-day lead) indicates a shift in the wind-speed-forced moisture transport during extreme rainfall events (VIMT shift indicated by Figure 4e,i, where lead minus 0-day is positive over the BoB and negative over the NEBI). Although, lower tropospheric moisture is

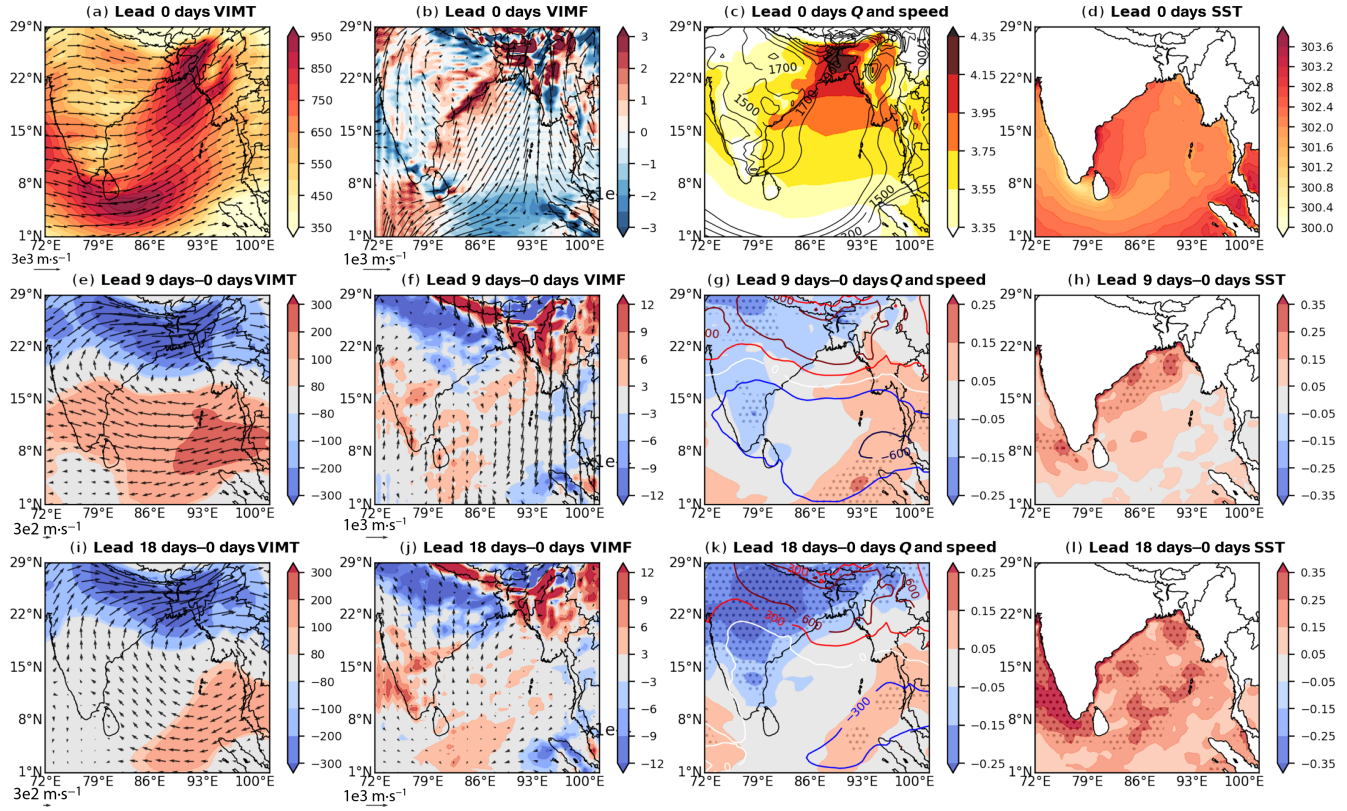

FIGURE 4 Composite mean from Modern-Era Retrospective Analysis for Research and Applications, Version 2 reanalysis of the 1-day extreme events (0-day lead, indicating onset day of extreme events) for (a) vertically integrated moisture transport (VIMT; shaded, unit: $kg{\cdot}kg^{-1}$) and vertically integrated wind (vector, unit: $m{\cdot}s^{-1}$), (b) vertically integrated moisture flux convergence (VIMF; unit: $s^{-1}\cdot kg{\cdot}kg^{-1}$) and vertically integrated wind convergence (vector, unit: $m{\cdot}s^{-1}$) (blue indicates divergence, and red indicates convergence), (c) specific humidity Q (shaded; unit: $kg{\cdot}kg^{-1}$) and vertically integrated wind speed (unit: $m{\cdot}s^{-1}$) (contoured), and (d) sea-surface temperature (SST; K). Difference between ninth day lead (9 days before the onset day) and 0-day lead for (e) VIMT, (f) VIMF, (g) Q (shaded) (unit: $kg{\cdot}kg^{-1}$) and vertically integrated wind speed (unit: $m{\cdot}s^{-1}$) (contoured, blue negative, white zero, and red positive), and (h) SST. Difference between 18th day lead (18 days before the onset day) and 0-day lead for (i) VIMT, (j) VIMF, (k) Q (shaded) and vertically integrated wind speed (contoured, blue negative, white zero, and red positive), and (l) SST (K). Significance for difference plots are stippled for (g), (h), (k), and (l), and only significant values are plotted for (e), (f), (i), and (j) to keep figures more clarified to read at 95% level using *t*-test.

more readily available, the sudden wind increase in the northern BoB and decrease in the southern BoB over a short period of time primarily contributes to the intense VIMT and VIMF that lead to extreme rainfall events over the NEBI region (Figure 4c,g,k). Though VIMT illustrates the amount of moisture transported, VIMF indicates the flux of moisture, signifying the source of moisture and convergence zones where moisture is converted to precipitation. The vertically integrated wind vector depicted in Figure 4a provides insight into the composite mean atmospheric circulation. This allows us to observe changes in atmospheric circulation over lead time, as evident in Figure 4e,i. The wind vector anomaly in these figures highlights an anticyclonic circulation pattern over the BoB, which contributes to moisture transport towards the north. Figure 4c represents specific humidity Q and wind speed V independently, as changes in either can influence the moisture transport to NEBI, resulting in extreme precipitation changes. The wind speed is represented by contour lines, showing that variations in both wind speed and moisture content collectively contribute to extreme events over NEBI.

The evolution of the composite mean SST shows that the BoB SST is warmer before 9-days and 18-days lead compared with the onset day of the extreme events (Figure 4d,h,l). This suggests that a relatively warmer SST during the 18-days and 9-days lead contributes to increased moisture over the BoB lower troposphere and serves as a source of moisture for extreme events over the NEBI. Subsequently, this moisture swiftly transports to the NEBI region due to a sudden increase in the LLJ, which is associated with the wind shift towards the northern BoB. Notably, the SST difference is more pronounced between the 18-days and 0-day lead (Figure 4l) than between the

9-days and 0-day lead (Figure 4h). This implies there might be a potential for predicting extreme rainfall events 9 to 18 days in advance based on the BoB SST.

Figure 5a,b shows the time series of the daily variability (black line) and frequency of daily extreme events (blue line) of the northern BoB VIMT (averaged over longitude 87° E–93° E and latitude 15° N–25° N) and SST (averaged over latitude 15° N–19° N, and BoB longitude that covers sea surface) during MJJASO. The daily variability of a season (MJJASO) is determined by taking the standard deviation of daily VIMT over the designated region across all days in that season, and it is calculated individually for each year. The trend in daily variability exhibits a consistent rise in temperature with the increasing trend of the seasonal mean SST and VIMT (Figure 5c). The increasing trend of the VIMT variability intensifies the frequency of extreme moisture transport to inland Bangladesh and northeast India due to both increased LLJ wind speed and lower tropospheric moisture in the atmosphere during the summer monsoon season. A coherent increase in the SST variability and frequency of extreme daily warming events of the northern BoB SST is also present over this period (Figure 5b). We discuss this further in Section 3.3, focusing on the contribution of increased moisture versus increased LLJ wind variability on the moisture transport and extreme NEBI rainfall events.

The low-pressure systems associated with monsoon depressions and tropical cyclones over the BoB can also lead to extreme rainfall events in Bangladesh and India (Krishnamurthy & Ajayamohan, 2010; Mooley, 1973; Roxy et al., 2017). However, Figure 5d shows that the frequency of depression and tropical cyclone systems decreases significantly during 1950–2021 over the BoB (Vishnu et al., 2016). Studies have shown that the BoB cyclonic storms decrease under climate change, most likely due to decreased variability of the tropical easterly jet relaxation episodes (Fahad et al., 2023). Hence, increased extreme rainfall events over these regions are not associated with cyclonic storms.

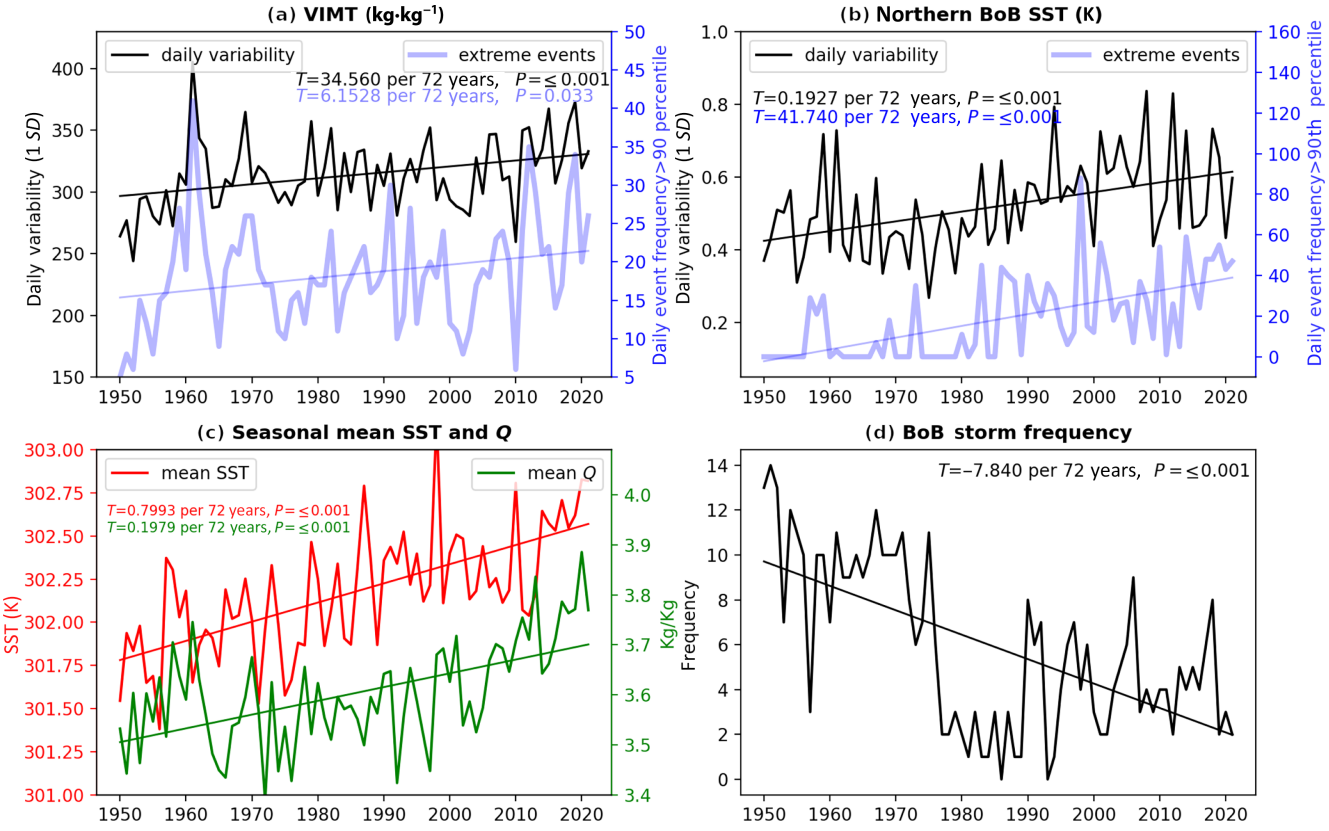

FIGURE 5 (a) May–October (MJJASO) vertically integrated moisture transport (VIMT) 700–1,000 hPa daily variability (1*SD*, black line) and frequency of extreme daily events >90th percentile (blue line; unit: kg·kg^{-1}) average taken over longitude 87° E–93° E and latitude 15° N–25° N. (b) MJJASO northern Bay of Bengal (BoB) sea-surface temperature (SST) 700–1,000 hPa daily variability (black line) and frequency of extreme daily events >90th percentile (blue line; unit: kg·kg^{-1}) average taken over longitude 87° E–93° E and latitude 15° N–19° N. (c) Seasonal mean SST and specific humidity *Q* time series. (d) MJJASO BoB storm frequency, including depression and tropical cyclones.

3.2 | CMIP6 future projections

The historical simulations (years 1950–1979) of downscaled CMIP6 MMM extreme rainfall events show a comparable annual climatology to observed data (Figures 6a,b and 1d, and Supporting Information Figures S2 and S3). The NEBI (Sylhet division of Bangladesh and Meghalaya Plateau of India) receives the largest extreme rainfall events, along with the SEB (Chittagong). The CMIP6 MMM future projection (SSP5-85, years 2050–2079) shows that the number of 1-day events increases significantly over NEBI (Figure 6a–c). The frequency of the 1-day events nearly doubles annually (increases frequency by ~10) over the NEBI region.

The zonal mean seasonal cycle of the changes between SSP5-85 and historical shows that the frequency of a 1-day event increases during the peak summer monsoon (June–August; Figure 6e). The zonal mean seasonal cycle of the ratio, calculated by dividing future projection (2050–2079) climatology by historical (1950–1979) climatology as a function of latitude, shows that the 1-day events quadruple over the NEBI and SEB (Figure 6f) during the peak summer monsoon season (June–August) in the future climate compared with historical simulations in 100 years. The future increase in the frequency of extreme events is associated with the summer monsoon season, when the climatology of extreme rainfalls is also at its maximum (primarily frequent during MJJASO) (Figures 6d,e and 3).

To understand what drives the increased frequency of extreme rainfall events in the future climate, we are showing results for the MJJASO months, when extreme rainfall events are mostly changed under global warming (Figure 6e,f). We have also explored the mechanism by separating months into pre-monsoon (April–May), monsoon (June–August), and post-monsoon

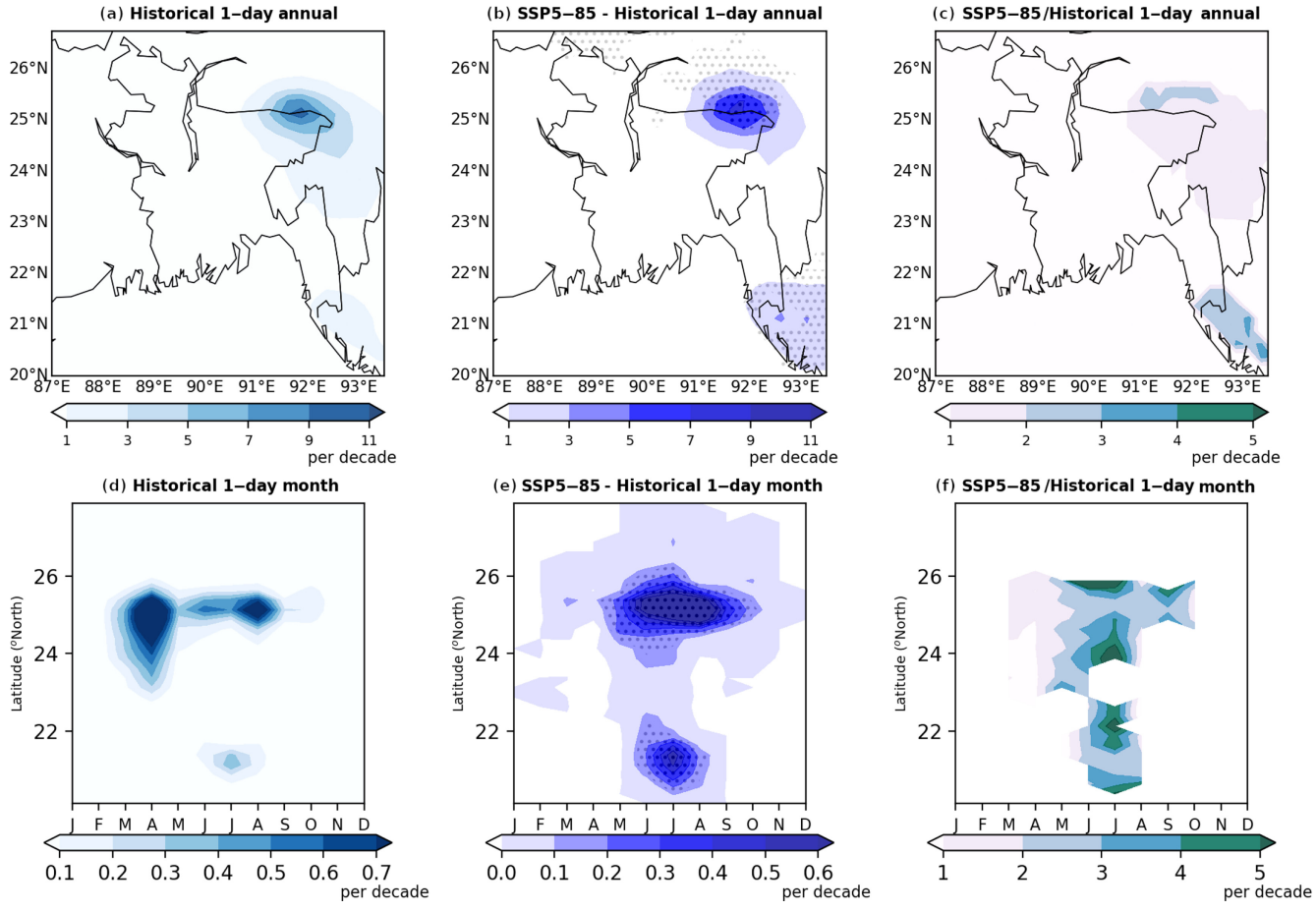

FIGURE 6 Coupled Model Intercomparison Project phase 6 multi-model mean: frequency of annual mean 1-day rainfall events (at least 150 mm·day^{-1}) per decade for (a) historical, (b) SSP5-85 minus historical, and (c) SSP5-85/historical ratio. (d) The seasonal cycle of the zonal mean (90° E–93° E) 1-day events. (e) The difference between SSP5-85 and the historical seasonal cycle difference and (f) SSP5-85/historical ratio for 1-day events. Stipplings are added to the difference of mean plots at 95% significance level for 12 models sample using two-sided Student's *t*-test.

(September–October) and found similar results and the same conclusion (figures not shown).

The MJJASO mean VIMT shows a significant increase from over the BoB to Bangladesh and northeast India in the future climate. The transport of moisture associated with the LLJ in the lower troposphere intensifies along with increased moisture convergence over the NEBI (Figure 7a,e,b,f). The VIMF shows that divergence over the southern BoB intensifies in the future climate, where climatologically the BoB acts as a source of moisture for extreme rainfall events. Climatologically, the VIMF is strongest during summer months due to local mountains forcing a strong LLJ to converge over that region, contributing to the mean rainfall. The intensified VIMF over NEBI indicates increased mean summer monsoon rainfall over this region, which is consistent with the increase in extreme rainfall events. During MJJASO, the moisture is mostly available over the northern BoB to NEBI region, which gets further transported and converged near the Meghalaya Plateau and Himalaya foothills in the future climate (Figure 7c,g). The difference between SSP5-85 and historical simulation shows the vertically integrated lower tropospheric moisture increases, especially over central India and western Bangladesh, whereas the wind speed associated with the LLJ increases near the northern BoB that contributes to the VIMT and VIMF (Figure 7g). The lower tropospheric moisture increase is consistent with the BoB SST warming in a future climate as a result of the Clausius–Clapeyron relation (Figure 7d,h). This result is also consistent with the general understanding that the moisture content in the troposphere increases under global warming conditions and the horizontal moisture transport intensifies, which contributes to the summer monsoon rainfall (Held & Soden, 2006).

The lower tropospheric moisture content in the BoB is more readily available, and the wind speed is slightly increased in the northern BoB in the future climate during MJJASO, contributing to the climatological monsoon rainfall (Figure 7c,g). However, an increase of extreme rainfall events will be possible when the events of lower tropospheric moisture content transport in a very short time-scale (~1–5 days) also increase. To understand this, we further analyzed the CMIP6 MMM

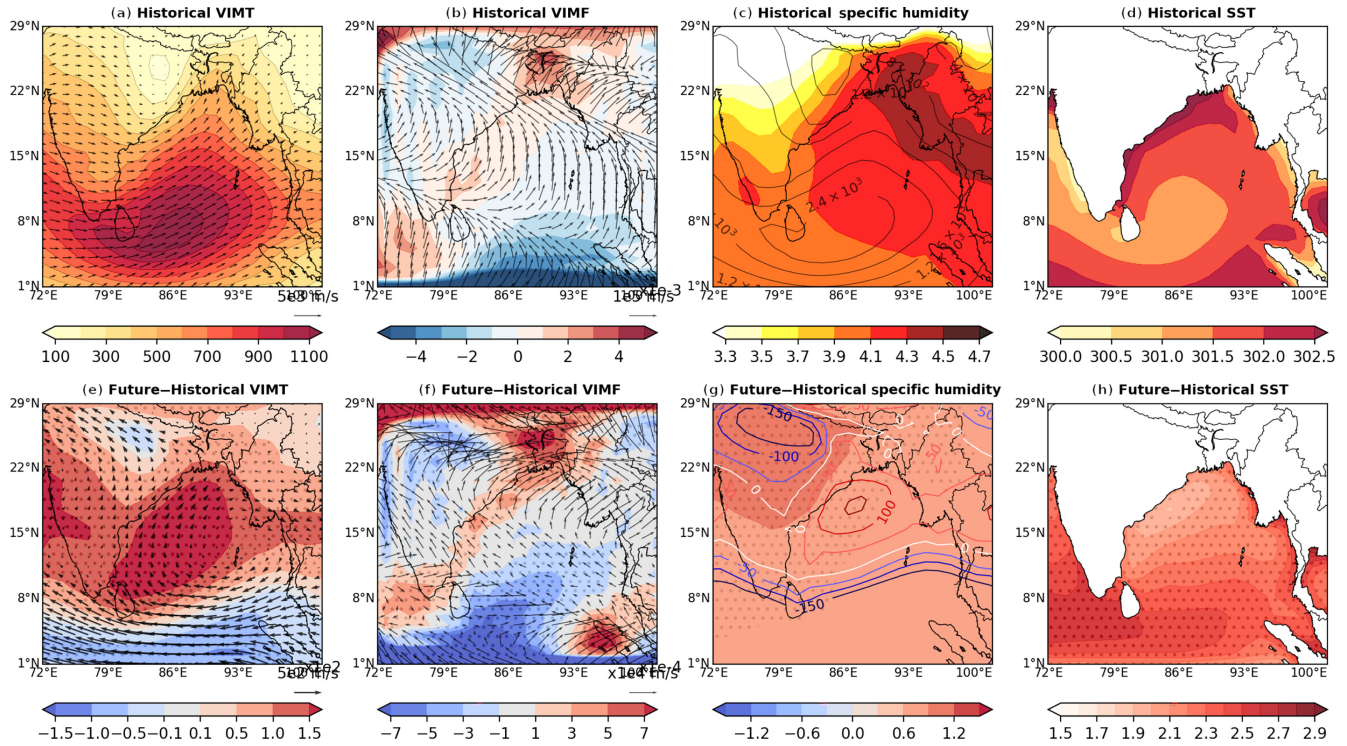

FIGURE 7 Coupled Model Intercomparison Project phase 6 May–October multi-model mean: climatological mean for (a) historical vertically integrated moisture transport (VIMT; shaded, unit: kg·kg^{-1}) and vertically integrated wind (1,000–700 hPa; vector, unit: m·s^{-1}), (b) historical vertically integrated moisture flux convergence (VIMF; convergence is positive; unit: s^{-1} ·kg·kg^{-1}) and vertically integrated convergence wind components (vector, unit: m·s^{-1}), (c) vertically integrated historical lower tropospheric specific humidity (shaded, unit: kg·kg^{-1}) and vertically integrated wind speed (contoured blue; unit: m·s^{-1}), and (d) historical sea-surface temperature (SST; unit: °C). (e)–(h) The corresponding difference between SSP5-85 and historical. The difference between SSP5-85 and historical plots are stippled at 95% significance level using Student's *t*-test.

daily variability of the LLJ wind and compared the variability between SSP5-85 and historical simulations (Figure 8).

To understand the behavior of the daily moisture events, we investigate the distribution of the moisture transport mean taken over the northern BoB to inland Bangladesh and India where the MJJASO mean LLJ wind increases in the future climate (Figure 8a). Figure 8b shows a histogram of the frequency of maximum daily 850 hPa moisture transport events (wind speed multiplied by specific humidity) over the northern BoB (region shown as a box in Figure 8a) for CMIP6 SSP5-85 and historical simulations, whereas Figure 8c shows a zoomed-in version of Figure 8b on the extreme end of the distribution tail. The frequency of extreme moisture transport events increases significantly in the future climate (Figure 8c). The frequency of extreme moisture transport events greater than 2.5 standard deviations (>98.76%) of CMIP6 models sampled data increases 4.03 times in 30 years in the SSP5-85 compared with historical simulation (Figure 8c). The quadrupled magnitude of the tropospheric moisture content with increased extreme LLJ wind speed events and northern BoB SST is consistent with the extreme rainfall event increase in the future climate under global warming conditions (Figure 8d–f).

3.3 | Dynamic versus thermodynamic forced change

The mean and extreme rainfall changes under a warmed climate can be due to a change in the atmospheric circulation, which is known as the "dynamic" component, or changes in the atmospheric moisture content (in response

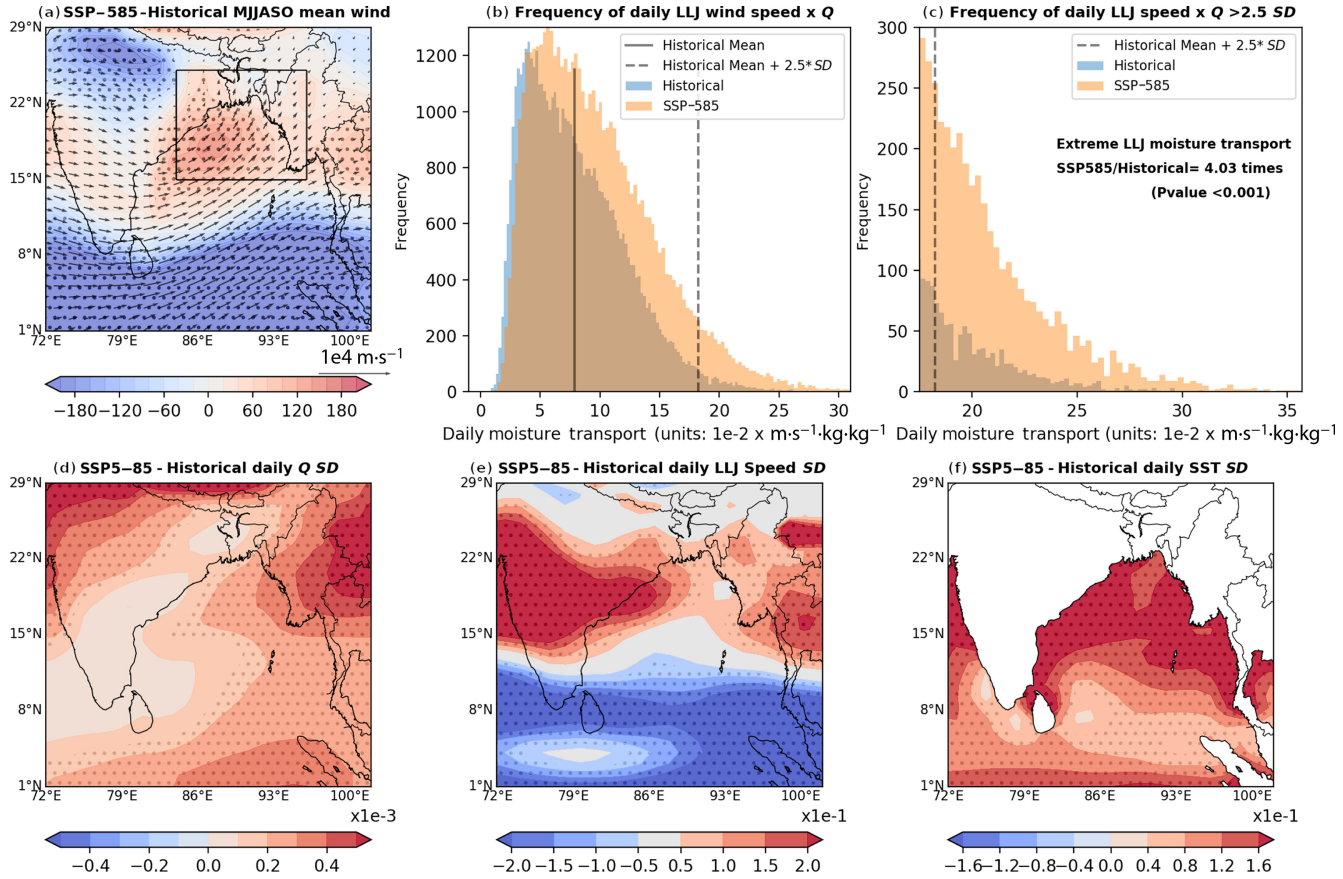

FIGURE 8 Coupled Model Intercomparison Project phase 6 (CMIP6) May–October (MJJASO): (a) historical vertically integrated wind (1,000–700 hPa) as a vector and SSP5-85 minus historical shaded, (b) daily frequency of maximum 850 hPa wind speed times specific humidity Q (units: $m \cdot s^{-1} \cdot kg \cdot kg^{-1}$) events over the northern Bay of Bengal in all CMIP6 models (region shown as a box in (a)) for historical (blue), SSP5-85 (orange) (overlapped areas are in brown). (c) Same as (b), but the distribution figure is zoomed in 2.5*SD* and greater. (d) Historical CMIP6 multi-model mean (MMM) standard deviation of daily 850 hPa specific humidity (unit: $kg \cdot kg^{-1}$). (e) SSP5-85 minus historical CMIP6 MMM standard deviation of daily 850 hPa wind speed (unit: $m \cdot s^{-1}$). (f) SSP5-85 minus historical CMIP6 MMM standard deviation of daily sea-surface temperature (SST; unit: K). For the difference of means plot, grids are stippled at 95% significance level. LLJ: low-level jet.

to temperature variations) known as the "thermodynamic" component. Owing to climate change and SST increase, there is more moisture available via evaporation, and the atmosphere can hold more moisture and heat content, which can in turn increase the mean and extreme rainfall events as a thermodynamic term (Emori & Brown, 2005; Pall et al., 2007). Meanwhile, changes in the atmospheric circulation can transport moisture that influences rainfall as a dynamic term.

The reanalysis data showing an increase in the VIMT from 1950 to 2021 over the BoB (Figure 5) is consistent with both linear increases in the lower tropospheric moisture content and changes in the atmospheric circulation associated with the LLJ. The projected changes in the CMIP6 simulation also show an increase in atmospheric moisture content due to increased SST, and the LLJ circulation intensifies over the northern BoB in the SSP5-85 (2050–2079) compared with historical (1950–1979) (Figures 7 and 8). However, to understand what drives the extreme precipitation change over NEBI, we need to separate the contributions of dynamic and thermodynamic terms.

In order to diagnose dynamic versus thermodynamic drivers of observed extreme rainfall events, we relate the occurrence of extreme 1-day widespread rainfall events over Meghalaya with circulation and moisture from ERA-5 over the period of 1950–2021. The 1-day mean 850 hPa meridional wind speed (V850), 500 hPa vertical velocity (W500), and total column-integrated water vapor (TCWV) are averaged over a local region along the southeastern slope of the Meghalaya Plateau (91° E–93° E and 25° N–25.25° N). V850 and W500 help differentiate the relationship between wind circulation change and extreme precipitation, indicating dynamical influence. Meanwhile, the relationship with TCWV helps us understand the influence of thermodynamic terms. A logistic regression (LR) model is constructed using V850, W500, and TCWV separately as predictors for the probability of occurrence of rainfall exceeding 150 mm in a day; see Equation (A.1). Figure 9a shows the interannual frequency of 1-day extreme events during MJJASO (red line, same as Figure 2a,d), along with the trend explained by the V850, TCWV, and W500 locally (same grid points). Only for Figure 9a, the daily LR model is used for variables locally to predict the occurrence of an event each day, then the predicted probability of events is summed each year and a trend is taken independently for V850, TCWV, and W500. Figure 9a further shows that V850 and W500 do not explain much interannual variability; however, they do predict moderate negative trends, whereas the trend predicted by TCWV is positive and explains about 20% of the observed trends in extreme rainfall events. This suggests that the trend in extreme events is partly driven thermodynamically by local moistening and not by local dynamics.

However, further examination leading up to extreme events shows enhanced wind speeds a week or more prior over the southwestern BoB, and apparent northward propagation possibly related to the monsoon active–break cycle. This is also evidenced by the presence of large-scale ascent over Bangladesh and descent over the BoB (Figure 9b). The daily LR between widespread extreme 1-day events of Meghalaya and the spatial map of W500 shows that there is a strong proportional relationship between the large-scale atmospheric circulation over the southern BoB 1 day prior to the extreme events (Figure 9b). Figure 9b shows marginal effects calculated from the coefficient of daily LR, indicating the likelihood of a daily extreme rainfall event occurring over the NEBI based on 1 unit W500 (unit: $Pa{\cdot}s^{-1}$) changes spatially (see appendix A for details). The marginal effect reveals the sensitive regions over the BoB and surrounding region of Meghalaya where changes in the atmospheric circulation play an important role in the occurrence of NEBI extreme rainfall events. The relation between W500 and the NEBI is, however, related to descending motion over the BoB and ascending motion over the surrounding region of NEBI (figure not shown). The composite mean meridional wind speed at 850 hPa (V850) during the 1-day events further demonstrates how the source of moisture over the BoB and the precipitation zone over the NEBI is connected through the LLJ, creating a moisture corridor. The result further indicates that, owing to remotely dynamically forced changes, the moisture flux and extreme 1-day rainfall events have increased over the NEBI in recent decades, whereas the local thermodynamic process also plays a significant role in the trend. This is consistent with the positive trend in northward winds and moisture flux over the BoB into Bangladesh (Figure 5a–c). Thus, it is likely that the local trend in moistening is due to enhanced advection of moisture from the BoB, which is related to both dynamic and thermodynamic changes. Owing to internal variability, capturing the relation with dynamic changes in observed data may be difficult due to its characteristic nature. The results are also consistent with recent findings (Allan et al., 2020; Zaitchik et al., 2023), where researchers concluded that, owing to a warming climate, more moisture flux increases regionally as a result of wind pattern and atmospheric circulation change, which amplifies the wet- and dry-season events.

We further analyzed CMIP6 models to identify the influence of dynamic and thermodynamic components. Figure 9c,d shows a correlation between the change in 1-day extreme rainfall events change (SSP5-85 – Historical) and the changes in LLJ wind speed (Figure 9c)

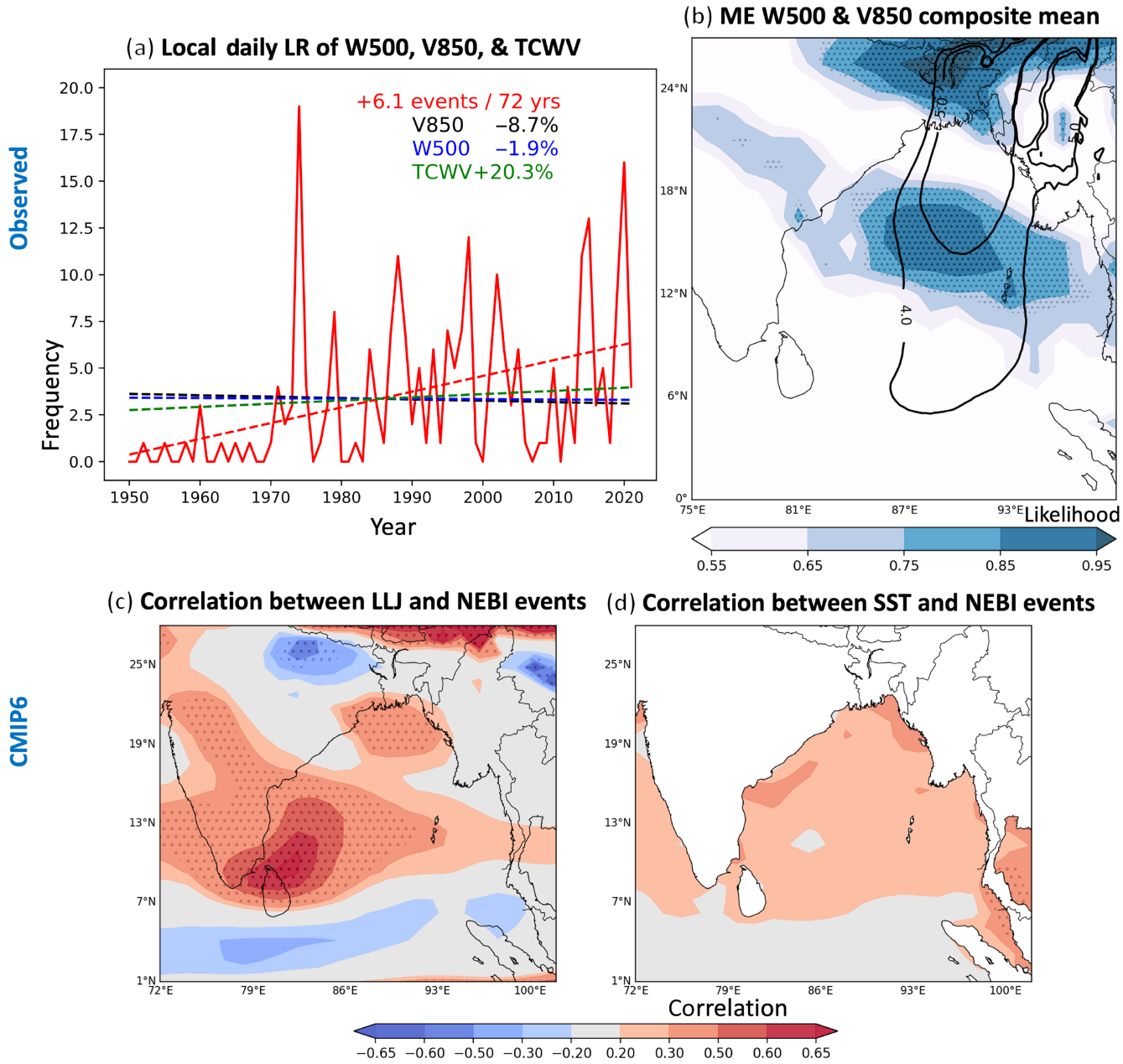

FIGURE 9 (a, b) Observed trend analysis. (c, d) Coupled Model Intercomparison Project phase 6 (CMIP6) model analysis. (a) May–October (MJJASO) observed 1-day widespread Meghalaya events (red, same as Figure 3a) and linear trend (dashed line). Percentage of extreme event trends that are explained by local meridional wind at 850 hPa (V850), local vertical velocity at 500 hPa (W500), and local total column water vapor (TCWV) determined through logistic regression (LR) models are shown in black, blue, and green lines. (b) The likelihood of extreme events occurring if one unit of W500 (unit: $Pa \cdot s^{-1}$) changes, determined through the marginal effect (ME) of LR (shaded color). Also shown is the composite mean V850 (unit: $m \cdot s^{-1}$; black contoured) during extreme events that show a connection from the northern Bay of Bengal to northeast Bangladesh and India (NEBI). (c, d) CMIP6 MJJASO seasonal mean intermodel spread: correlation between NEBI 1-day extreme rainfall events change (future minus historical) and low-level jet (LLJ) wind circulation (850 hPa) change (future minus historical) in (c) and sea-surface temperature (SST) change in (d). Significant correlation explains what drives the intermodel spread of the NEBI extreme event change under global warming.

and SST (Figure 9d) across CMIP6 models. The high correlation (~0.7; similar magnitude or relation found from observed data analysis, Figure 9b) between the change in LLJ wind speed and extreme events in NEBI shows that the intermodel spread of CMIP6 extreme events is related to the intermodel spread of the southeastern BoB LLJ wind speed change. In contrast, the correlation between the northern BoB SST and extreme events in

NEBI shows no significant correlation, indicating that the primary role in increasing extreme events under global warming conditions is played by the remote dynamical forcing. This further confirms the critical role that the remote dynamical forcing plays on the NEBI extreme rainfall event change under global warming conditions, which is consistent with the observed and reanalysis data.

4 | DISCUSSION

Along with the increasing trend of flash-flood-causing extreme rainfall events, extreme events have been getting more intense over the last decades in the NEBI region (Figures 1,2, and 3). On June 17, 2022, Cherapunji of Meghalaya Plateau received the third highest 1-day rainfall (972 mm·day^{-1}), whereas the highest ever recorded 1-day rainfall was in June 1995 (1,563.3 mm·day^{-1}). In 2022, there were two consecutive extreme rainfall and associated flooding events over the NEBI from May to June (Figure 10a,b). The intense rainfall events have caused the Surma–Kushiyara river basin to overflow, inundating most of the nine districts in the northeastern part of Bangladesh. The most severe and damaged conditions were in Sylhet (84% submerged area) and Sunamganj (94% submerged area) (Figure 10c,d). During the May–June 2022 period, more than 80 people died and 244,060 ha of crops, 40,000 tube wells, and about USD 28.1 million worth of livestock were damaged due to flash floods (DGHS, 2022). The CMIP6 future projection shows extreme events like this will be more frequent in the future.

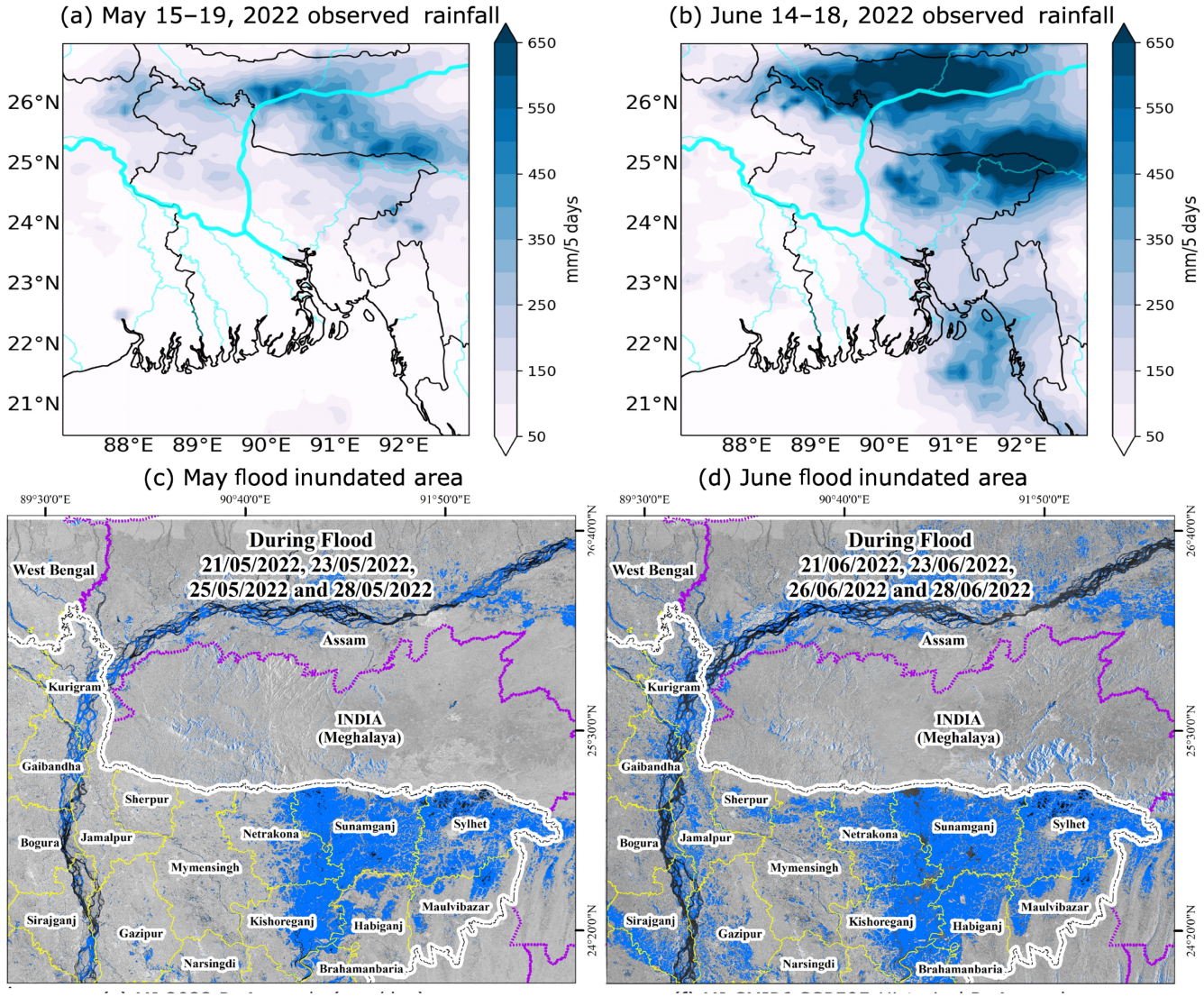

FIGURE 10 May–June 2022 flooding event showing 5 days of cumulative rainfall for (a) May 15–May 19 and (b) June 14–June 18 (from IMERG data); (c) May and (d) June flood inundated area.

The SST modes, such as ENSO and the IOD, play an important role in mean summer monsoon rainfall and extreme rainfall events over Bangladesh and India (Chowdhury & Ward, 2007; Ihara et al., 2007). With increasing global warming, both the mean state and variability of SST increase in both the tropical Indian Ocean and the Pacific Ocean, which can potentially influence rainfall variability over NEBI and SEB (Cai et al., 2023; Fahad & Burls, 2022). Roxy et al. (2017) found the changes in the extreme events in central India are dynamic component driven even though the moisture increase is significant over the Indian Ocean, which is consistent with our findings for the NEBI region and the BoB.

During the onset day of extreme rainfall events, the BoB SST anomaly creates a temperature gradient from the warmer northern BoB to the colder mid-southern BoB. Although, the BoB SST warming in the future climate increases everywhere, it creates a stronger opposite SST gradient (warm northern BoB to warmer southern BoB SST) during the MJJASO mean. The sudden intensification episode of the LLJ over the BoB increases in the future, which contributes to the increase in extreme rainfall events, even though the mean SST gradient is opposite compared with the onset day SST anomaly gradient. This infers that the mean SST gradient potentially plays a non-significant role in the intensification of LLJ episodes under global warming.

A few caveats also need to be considered here. The observed extreme rainfall and mean seasonal rainfall events exhibit large interannual variability over Meghalaya, specifically in Cherrapunji (Figure 3a). It is very important to use a longer dataset over this region to understand the trend, as investigating only 20–30 years of data may lead to erroneous conclusions. The variability of 1-day extreme rainfall events over Meghalaya in IMD data increased after the 1970s (Figure 3a). This change in the extreme rainfall events' variability after the 1970s is, however, consistent with the mean seasonal rainfall over Meghalaya (Figure 3a, black line), daily variability of BoB SST warming and extreme SST warming events (Figure 5b), MJJASO seasonal mean SST warming and specific humidity trend (Figure 5c). Weaker BoB SST warming and available moisture variability over the BoB in the 1950s–1970s contributed to the seasonal mean rainfall and extreme events over Meghalaya. To reduce uncertainty in the IMD dataset for Meghalaya, we have used widespread events for extreme rainfall events, defined as a rainfall event that exceeds 150 mm in a day and covers at least 200 km^2 of the area in Meghalaya (Figure 3a). To validate the trend, we also used APHRODITE gridded observed data (years 1951–2015). Owing to relatively low-resolution processed gridded data and a shorter time range compared with IMD (1950–2021), APHRODITE and IMD show discrepancies in the extreme event trend over eastern Meghalaya. We further compared ERA-5 data to validate the extreme event trends and ratio over the years 1950–2021 and found a similar quadruple increase of extreme events over the NEBI and SEB (Supporting Information Figure S1). A change in the rain-gauge network can potentially contribute to the rainfall trends. However, prior studies have validated and used the same IMD dataset that incorporates more than 3,100 stations per day with fixed rain-gauge data and satellite data (Pai et al., 2015; Rajeevan et al., 2008; Roxy et al., 2017).

The CMIP6 MMM exhibits a dry bias relative to observed climatology, leading to reduced mean climatological precipitation and fewer 150 mm 1-day extreme rainfall events than observed data (Figure 6, and Supporting Information Figures S2 and S3). When compared with APHRODITE data, the CMIP6 MMM historical 1-day extreme events climatology indicates that there are fewer 1-day events in the CMIP6 models, and their maxima are shifted towards eastern Meghalaya. In contrast, the observed APHRODITE data places 1-day extreme rainfall events more centrally around eastern Meghalaya. The latest high-resolution CMIP6 models still exhibit variability in the intermodel spread for 1-day events. The pronounced discrepancies in extreme events and mean seasonal rainfall, when compared with observed data, are likely attributed to biases in the LLJ, SST, and moisture transport. This is further compounded by the relatively lower spatial resolution that potentially struggles to accurately resolve convective precipitation. However, despite this variability, all models consistently show similar changes in extreme rainfall events in the context of global warming, signifying a uniform response to climate change over Bangladesh and India. The alignment between the observed trend and the CMIP6 future projections suggests that the models accurately represent changes in extreme rainfall events with a high degree of fidelity.

5 | SUMMARY

The monsoon extreme rainfall-related flood events are very frequent over NEBI (Sylhet, Assam) and SEB (Chittagong division). Extreme rainfall events over these regions are associated with the summer monsoon rainfall starting from May to October. The rainfall over the Meghalaya Plateau contributes to the heavy flash flood events over the NEBI frequently during monsoon season.

The observed trend of the 1-day extreme rainfall events (>150 $mm \cdot day^{-1}$) shows a nearly quadrupled frequency over the Meghalaya Plateau and surrounding regions (especially over the eastern Meghalaya) during MJJASO,

from 1950 to 2021 compared with the first 30 years of baseline. The increase in extreme events is consistent with the quadruple increase in flash flood events over the Sylhet region (northeastern Bangladesh) during the same period. The APHRODITE data further show that the increasing trends in extreme rainfall events extend to the Sylhet region of Bangladesh and the coastal area of Chittagong (SEB), which is not evident from a single station of BMD data.

Focusing on NEBI, where extreme rainfall events and flood events are the most frequent and primary concern, we found a warm SST anomaly over the northern BoB plays an important role in providing the source of moisture, whereas a sudden intensification episode of the LLJ over the northern BoB carries moisture over short periods of time (~1–5 days) near the Meghalaya Plateau, and finally leading to extreme rainfall events forced by the local high topography. This dynamical mechanism is consistent with the mechanism of mean monsoonal rainfall over the same region (Fahad et al., 2022). The CMIP6 MMM future projection shows that extreme rainfall events quadruple over the NEBI and continue to increase over the SEB in 2050–2079 compared with 1950–1979. The seasonal cycle of extreme events is also projected to start early in pre-monsoon and late end of the post-monsoon season.

The CMIP6 MMM MJJASO seasonal mean shows the vertically integrated lower tropospheric moisture transport increases from the northern BoB to northeastern Bangladesh, along with an intensified moisture divergence and strong convergence increase over the Meghalaya Plateau that contributes to the intensified summer monsoon rainfall. This is due to both seasonal mean increased humidity and a shift in the BoB LLJ towards the north. The SST also increases all over the BoB, including the northern BoB. This is consistent with extreme rainfall dynamical mechanisms. However, extreme rainfall events are due to intensified LLJ speed episodes in a short time-scale. We further found that the daily variability of the LLJ increases over the northern BoB (more unstable), whereas it decreases over the mid to southern BoB (more stable) in CMIP MMM future projection. The frequency of extreme daily maximum episodes of moisture transport greater than 2.5 standard deviations associated with the LLJ over the northern BoB is quadrupled in the future climate (2050–2079) compared with historical simulation (1950–1979), which is very consistent with the increase in extreme rainfall events.

After further investigation of the influence of dynamic versus thermodynamic forcing on the extreme rainfall events change, we found that the thermodynamic process plays a crucial role locally over the NEBI through increased moisture in the atmosphere. However, the moisture over the NEBI is transported through a dynamic process of changed circulation associated with the LLJ over the BoB. This is very consistent with the observed extreme rainfall events change in CMIP6 MMM future projection. The lag–lead relation between extreme rainfall over the NEBI and SST over the BoB suggests strong potential for extreme rainfall event predictability exists even 9 to 18 days before the onset day.

Given that Bangladesh and India have the highest population densities in the world, and natural disasters like flash floods and landslides are very common due to frequent extreme rainfall events, it is crucial to improve the local extreme event warning systems. This article potentially serves the purpose of discussing what generally drives the extreme rainfall events over this region, how the extreme rainfall has changed over the last decades using observed station data, how it will further change using CMIP6 high-resolution downscaled multi-model data, and finally what are the dynamic versus a thermodynamic processes that contribute to the increased extreme rainfall events under global warming conditions.

AUTHOR CONTRIBUTIONS

Abdullah A. Fahad came up with the idea, wrote the manuscript, and created Figures 1a, 2 through 8, as well as 9(b,c,d), and conducted all the relevant analysis. **Mahdi Hasan** created Figures 1a(c,d) and 10(a,b). **Noshin Sharmili** created Figure 1b and contributed to the writing of the discussion section. **Shammunul Islam** provided BMD data, and created Figures 10(c,d). **Erik T. Swenson** created Figure 9(a). **M. K. Roxy** provided IMD data and reviewed the manuscript. Logistic regression calculation was conducted by E Swenson. Marginal Effects calculation was conducted by A Fahad. All authors contributed to the discussion of the manuscript's concept.

ACKNOWLEDGEMENTS

We gratefully acknowledge the use of high-end computer resources at NASA's Computer Center for Climate Simulation (NCCS) Discover. The utilization of downscaled CMIP6 high-resolution data was made possible by NCCS. The MERRA-2 of the Global Modeling and Assimilation Office (GMAO) at NASA's Goddard Space Flight Center also accessed through the NCCS system. Our appreciation extends to the World Climate Research Programme's Working Group on Coupled Modelling, responsible for CMIP. We also thank the climate modeling groups (as listed in Table 1 of this article) for producing and sharing their model output. Further, we recognize the high-performance computing and analysis support

from Cheyenne, courtesy of NCAR's Computational and Information Systems Laboratory, sponsored by the NSF. Our thanks also go to European Centre for Medium-Range Weather Forecasts for providing the ERA-5 dataset.

CONFLICT OF INTEREST STATEMENT

No conflict of interests.

DATA AVAILABILITY STATEMENT

MERRA-2 reanalysis data are available online at https://gmao.gsfc.nasa.gov/reanalysis/MERRA-2/data_access/. ERA-5 data are available online at https://cds.climate.copernicus.eu/cdsapp#!/dataset/reanalysis-era5-single-levels?tab=overview. NCEP–NCAR Reanalysis is available online at https://psl.noaa.gov/data/gridded/data.ncep.reanalysis.html. BMD data can be accessed from https://www.bmddataportal.com/#/. IMD data can be accessed from https://dsp.imdpune.gov.in/. International Best Track Archive for Climate Stewardship: https://www.ncei.noaa.gov/products/international-best-track-archive. CMIP6 data can be accessed at https://esgf-node.llnl.gov/projects/cmip6/.

ORCID

Abdullah A. Fahad https://orcid.org/0000-0001-8238-8739
Mahdi Hasan https://orcid.org/0000-0001-8975-2900
Erik T. Swenson https://orcid.org/0000-0003-2901-5540

REFERENCES

Acharya, N., Faniriantsoa, R., Rashid, B., Sultana, R., Montes, C., Dinku, T. et al. (2020) Developing high-resolution gridded rainfall and temperature data for Bangladesh: the enacts-bmd dataset. Preprint. https://doi.org/10.20944/preprints202012.0468.v1

Agency, T.E.S. (2020) Sentinel-1. https://sentinels.copernicus.eu/web/sentinel/missions/sentinel-1

Ahasan, M., Chowdhary, M.A. & Quadir, D. (2010) Variability and trends of summer monsoon rainfall over Bangladesh. *Journal of Hydrology and Meteorology*, 7, 1–17. Available from: https://doi.org/10.3126/jhm.v7i1.5612

Ahmed, B. (2015) Landslide susceptibility mapping using multi-criteria evaluation techniques in Chittagong metropolitan area, Bangladesh. *Landslides*, 12, 1077–1095. Available from: https://doi.org/10.1007/s10346-014-0521-x

Ahmed, B. (2021) The root causes of landslide vulnerability in Bangladesh. *Landslides*, 18, 1707–1720. Available from: https://doi.org/10.1007/s10346-020-01606-0

Ahmed, M., Alam, M.S., Yousuf, A.H.M., Islam, M. et al. (2017) A long-term trend in precipitation of different spatial regions of Bangladesh and its teleconnections with el niño/southern oscillation and Indian ocean dipole. *Theoretical and Applied Climatology*, 129, 473–486. Available from: https://doi.org/10.1007/s00704-016-1765-2

Allan, R.P., Barlow, M., Byrne, M.P., Cherchi, A., Douville, H., Fowler, H.J. et al. (2020) Advances in understanding large-scale responses of the water cycle to climate change. *Annals of the New York Academy of Sciences*, 1472, 49–75.

Brouwer, R., Akter, S., Brander, L. & Haque, E. (2007) Socioeconomic vulnerability and adaptation to environmental risk: a case study of climate change and flooding in Bangladesh. *Risk Analysis: An International Journal*, 27, 313–326. Available from: https://doi.org/10.1111/j.1539-6924.2007.00884.x

Burls, N.J., Blamey, R.C., Cash, B.A., Swenson, E.T., Fahad, A.A., Bopape, M.-J.M. et al. (2019) The cape town "day zero" drought and Hadley cell expansion. *Npj Climate and Atmospheric Science*, 2, 1–8. Available from: https://doi.org/10.1038/s41612-019-0084-6

Cai, W., Ng, B., Geng, T., Jia, F., Wu, L., Wang, G. et al. (2023) Anthropogenic impacts on twentieth-century enso variability changes. *Nature Reviews Earth & Environment*, 4, 407–418.

Cameron, A. & Trivedi, P. (2010) *Microeconometrics using Stata (Vol. 2)*. College Station, TX: Stata Press.

Chowdhury, M.R. & Ward, M.N. (2007) Seasonal flooding in Bangladesh–variability and predictability. *Hydrological Processes: An International Journal*, 21, 335–347. Available from: https://doi.org/10.1002/hyp.6236

Danielson, J.J. & Gesch, D.B. (2011) *Global multi-resolution terrain elevation data 2010 (GMTED2010)*. US Geological Survey Washington, DC, USA: US Department of the Interior. https://pubs.usgs.gov/of/2011/1073/

DGHS. (2022) Directorate general of health services. http://dashboard.dghs.gov.bd/webportal/pages/flood_affected_situation.php

Doblas-Reyes, F., Sorensson, A., Almazroui, M., Dosio, A., Gutowski, W., Haarsma, R. et al. (2021) Linking global to regional climate change.

Douville, H., Raghavan, K., Renwick, J., Allan, R.P., Arias, P.A., Barlow, M. et al. (2021) Water cycle changes.

EMDAT. (2022) The international disasters database. https://www.emdat.be/emdat_db/

Emori, S. & Brown, S. (2005) Dynamic and thermodynamic changes in mean and extreme precipitation under changed climate. *Geophysical Research Letters*, 32, 1-5. Available from: https://doi.org/10.1029/2005GL023272

Eyring, V., Bony, S., Meehl, G.A., Senior, C.A., Stevens, B., Stouffer, R.J. et al. (2016) Overview of the coupled model intercomparison project phase 6 (cmip6) experimental design and organization. *Geoscientific Model Development*, 9, 1937–1958. Available from: https://doi.org/10.5194/gmd-9-1937-2016

Fahad, A.A. & Burls, N.J. (2022) The influence of direct radiative forcing versus indirect sea surface temperature warming on southern hemisphere subtropical anticyclones under global warming. *Climate Dynamics*, 58, 2333–2350. Available from: https://doi.org/10.1007/s00382-021-06006-1

Fahad, A.A., Burls, N.J. & Strasberg, Z. (2020) How will southern hemisphere subtropical anticyclones respond to global warming? Mechanisms and seasonality in cmip5 and cmip6 model projections. *Climate Dynamics*, 55, 703–718. Available from: https://doi.org/10.1007/s00382-020-05290-7

Fahad, A.A., Reale, O., Molod, A., Sany, T.A., Ahammad, M.T. & Menemenlis, D. (2023) The role of tropical easterly jet on the bay of Bengal's tropical cyclones: observed climatology and future projection. *Journal of Climate*, 36, 5825–5840 https://journals.ametsoc.org/view/journals/clim/36/17/JCLI-D-22-0804.1.xml

Fahad, A.A., Singh, B., Kamal, M., Ahmed, T., Kibria, M. & Chowdhury, N.R. (2022) The role of local topography and sea surface temperature on summer monsoon precipitation over Bangladesh and Northeast India. *International Journal of Climatology*, 42, 4564–4579. Available from: https://doi.org/10.1002/joc.7490

Gelaro, R., McCarty, W., Suárez, M.J., Todling, R., Molod, A., Takacs, L. et al. (2017) The modern-era retrospective analysis for research and applications, version 2 (merra-2). *Journal of Climate*, 30, 5419–5454. Available from: https://doi.org/10.1175/JCLI-D-16-0758.1

Hausfather, Z. & Peters, G.P. (2020) Emissions–the 'business as usual' story is misleading. *Nature*, 577, 618–620.

Held, I.M. & Soden, B.J. (2006) Robust responses of the hydrological cycle to global warming. *Journal of Climate*, 19, 5686–5699. Available from: https://doi.org/10.1175/JCLI3990.1

Hersbach, H. (2020) The era5 global reanalysis. *Quarterly Journal of the Royal Meteorological Society*, 146, 1999–2049. Available from: https://doi.org/10.1002/qj.3803

Huffman, G.J., Bolvin, D.T., Braithwaite, D., Hsu, K., Joyce, R., Xie, P. et al. (2015) Nasa global precipitation measurement (gpm) integrated multi-satellite retrievals for gpm (imerg). *Algorithm Theoretical Basis Document (ATBD) Version*, 4, 1-35.

Ihara, C., Kushnir, Y., Cane, M.A. & De La Peña, V.H. (2007) Indian summer monsoon rainfall and its link with enso and Indian ocean climate indices. *International Journal of Climatology: A Journal of the Royal Meteorological Society*, 27, 179–187. Available from: https://doi.org/10.1002/joc.1394

Islam, M.N. & Uyeda, H. (2007) Use of trmm in determining the climatic characteristics of rainfall over Bangladesh. *Remote Sensing of Environment*, 108, 264–276. Available from: https://doi.org/10.1016/j.rse.2006.11.011

Jamir, T., Gadgil, A.S. & De, U. (2008) Recent floods related natural hazards over west coast and Northeast India. *Journal of Indian Geophysics Union*, 12, 179–182.

Kalnay, E., Kanamitsu, M., Kistler, R., Collins, W., Deaven, D., Gandin, L. et al. (1996) The ncep/ncar 40-year reanalysis project. *Bulletin of the American Meteorological Society*, 77, 437–472. Available from: https://doi.org/10.1175/1520-0477(1996)077.CO;2

Knapp, K.R., Kruk, M.C., Levinson, D.H., Diamond, H.J. & Neumann, C.J. (2010) The international best track archive for climate stewardship (ibtracs) unifying tropical cyclone data. *Bulletin of the American Meteorological Society*, 91, 363–376. Available from: https://doi.org/10.1175/2009BAMS2755.1

Krishnamurthy, V. & Ajayamohan, R. (2010) Composite structure of monsoon low pressure systems and its relation to indian rainfall. *Journal of Climate*, 23, 4285–4305. Available from: https://doi.org/10.1175/2010JCLI2953.1

Krishnamurthy, V. & Shukla, J. (2000) Intraseasonal and interannual variability of rainfall over India. *Journal of Climate*, 13, 4366–4377. Available from: https://doi.org/10.1175/1520-0442(2000)0130.CO;2

Long, J. (1997) *Regression models for categorical and limited dependent variables*. Thousand Oaks, CA: Sage Publishing.

Mahanta, R., Sarma, D. & Choudhury, A. (2013) Heavy rainfall occurrences in Northeast India. *International Journal of Climatology*, 33, 1456–1469. Available from: https://doi.org/10.1002/joc.3526

Mia, M., Sultana, N. & Paul, A. (2015) Studies on the causes, impacts and mitigation strategies of landslide in Chittagong city, Bangladesh. *Journal of Environmental Science and Natural Resources*, 8, 1–5. Available from: https://doi.org/10.3329/jesnr.v8i2.26854

Mishra, A.K., Meer, M.S. & Nagaraju, V. (2019) Satellite-based monitoring of recent heavy flooding over north-eastern states of India in July 2019. *Natural Hazards*, 97, 1407–1412. Available from: https://doi.org/10.1007/s11069-019-03707-z

Mood, C. (2010) Logistic regression: why we cannot do what we think we can do, and what we can do about it. *European Sociological Review*, 26, 67–82.

Mooley, D.A. (1973) Some aspects of Indian monsoon depressions and the associated rainfall. *Monthly Weather Review*, 101, 271–280. Available from: https://doi.org/10.1175/1520-0493(1973)1013.CO;2

Murata, F., Terao, T., Fujinami, H., Hayashi, T., Asada, H., Matsumoto, J. et al. (2017) Dominant synoptic disturbance in the extreme rainfall at Cherrapunji, Northeast India, based on 104 years of rainfall data (1902–2005). *Journal of Climate*, 30, 8237–8251. Available from: https://doi.org/10.1175/JCLI-D-16-0435.1

Pai, D., Sridhar, L., Badwaik, M. & Rajeevan, M. (2015) Analysis of the daily rainfall events over India using a new long period (1901–2010) high resolution (0.25× 0.25) gridded rainfall data set. *Climate Dynamics*, 45, 755–776.

Pall, P., Allen, M. & Stone, D.A. (2007) Testing the clausius–clapeyron constraint on changes in extreme precipitation under CO2 warming. *Climate Dynamics*, 28, 351–363. Available from: https://doi.org/10.1007/s00382-006-0180-2

Phukon, P., Chetia, D. & Das, P. (2012) Landslide susceptibility assessment in the Guwahati city, Assam using analytic hierarchy process (AHP) and geographic information system (GIS). *International Journal of Computers and Applications Engineering Sciences*, 2, 1–6.

Power, S.B., Delage, F., Colman, R. & Moise, A. (2012) Consensus on twenty-first-century rainfall projections in climate models more widespread than previously thought. *Journal of Climate*, 25, 3792–3809. Available from: https://doi.org/10.1175/JCLI-D-11-00354.1

Rajeevan, M., Bhate, J. & Jaswal, A.K. (2008) Analysis of variability and trends of extreme rainfall events over India using 104 years of gridded daily rainfall data. *Geophysical Research Letters*, 35, 1-6.

Rimi, R.H., Haustein, K., Allen, M.R. & Barbour, E.J. (2019) Risks of pre-monsoon extreme rainfall events of Bangladesh: is anthropogenic climate change playing a role? *Bulletin of the American Meteorological Society*, 100, S61–S65. Available from: https://doi.org/10.1175/BAMS-D-18-0152.1

Rimi, R.H., Haustein, K., Barbour, E.J., Sparrow, S.N., Li, S., Wallom, D.C.H. et al. (2022) Risks of seasonal extreme rainfall events in Bangladesh under 1.5 and 2.0°C warmer worlds–how anthropogenic aerosols change the story. *Hydrology and Earth System Sciences*, 26, 5737–5756 https://hess.copernicus.org/articles/26/5737/2022/

Roxy, M.K., Ghosh, S., Pathak, A., Athulya, R., Mujumdar, M., Murtugudde, R. et al. (2017) A threefold rise in widespread extreme rain events over Central India. *Nature Communications*, 8, 1–11. Available from: https://doi.org/10.1038/s41467-017-00744-9

Sarker, A.A. & Rashid, A. (2013) Landslide and flashflood in Bangladesh. In: *Disaster risk reduction approaches in Bangladesh*.

New York City: Springer, pp. 165–189. Available from: https://doi.org/10.1007/978-4-431-54252-0_8

Schnase, J.L., Webster, W.P., Parnell, L.A. & Duffy, D.Q. (2011) The nasa center for climate simulation data management system. Paper presented at: 2011 IEEE 27th symposium on mass storage systems and technologies (MSST), 1–6. IEEE. https://ieeexplore.ieee.org/document/5937235

Seneviratne, S.I., Zhang, X., Adnan, M., Badi, W., Dereczynski, C., Di Luca, A. et al. (2021) Weather and climate extreme events in a changing climate. (chapter 11).

Shahid, S. (2011) Trends in extreme rainfall events of Bangladesh. *Theoretical and Applied Climatology*, 104, 489–499. Available from: https://doi.org/10.1007/s00704-010-0363-y

Tang, H., Wang, J., Hu, K., Huang, G., Chowdary, J.S., Wang, Y. et al. (2022) Increasing 2020-like boreal summer rainfall extremes over northeast indian subcontinent under greenhouse warming. *Geophysical Research Letters*, 49, e2021GL096377. Available from: https://doi.org/10.1029/2021GL096377

Thomas, M., Tellman, E., DeVries, B., Islam, A.S., Steckler, M., Goodman, M. et al. (2020) A framework to assess remote sensing algorithms for satellite-based flood index-insurance. In Review. https://doi.org/10.1109/JSTARS.2023.3244098

Thomas, N.P., Collow, A., Bosilovich, M. & Dezfuli, A. (2023) Effect of baseline period on quantification of climate extremes over the United States. GRL (Submitted).

Thrasher, B., Wang, W., Michaelis, A., Melton, F., Lee, T. & Nemani, R. (2022) Nasa global daily downscaled projections, cmip6. *Scientific Data*, 9, 1–6. Available from: https://doi.org/10.1038/s41597-022-01393-4

Vishnu, S., Francis, P., Shenoi, S. & Ramakrishna, S. (2016) On the decreasing trend of the number of monsoon depressions in the bay of Bengal. *Environmental Research Letters*, 11, 014011. Available from: https://doi.org/10.1088/1748-9326/11/1/014011

Wahiduzzaman, M. & Luo, J.-J. (2021) A statistical analysis on the contribution of el niño–southern oscillation to the rainfall and temperature over Bangladesh. *Meteorology and Atmospheric Physics*, 133, 55–68. Available from: https://doi.org/10.1007/s00703-020-00733-6

Yatagai, A., Kamiguchi, K., Arakawa, O., Hamada, A., Yasutomi, N. & Kitoh, A. (2012) Aphrodite: constructing a long-term daily gridded precipitation dataset for asia based on a dense network of rain gauges. *Bulletin of the American Meteorological Society*, 93, 1401–1415.

Zaitchik, B.F., Rodell, M., Biasutti, M. & Seneviratne, S.I. (2023) Wetting and drying trends under climate change. *Nature Water*, 1, 502–513.

SUPPORTING INFORMATION

Additional supporting information can be found online in the Supporting Information section at the end of this article.

How to cite this article: Fahad, A.A., Hasan, M., Sharmili, N., Islam, S., Swenson, E.T. & Roxy, M.K. (2024) Climate change quadruples flood-causing extreme monsoon rainfall events in Bangladesh and northeast India. *Quarterly Journal of the Royal Meteorological Society*, 150(760), 1267–1287. Available from: https://doi.org/10.1002/qj.4645

APPENDIX

In this study, LR was computed in Python using the sklearn library, and it was calculated using a standard L2 penalty. In LR, the relationship between the predictor and response variables is encapsulated by the logit function (Long, 1997):

$$\log\left(\frac{p}{1-p}\right) = \beta_0 + \beta_1 X_1 + \beta_2 X_2 + \cdots, \tag{A.1}$$

where log is the natural logarithm, p indicates the probability of the event occurring, $X_1, X_2, \ldots$ are the predictor variables, and $\beta_0, \beta_1, \ldots$ are the regression coefficients.

Marginal effects offer insights into the change in the predicted probability of the dependent variable due to a one-unit alteration in a predictor, considering all other variables are constant (Mood, 2010). For continuous predictors, the marginal effect of X_1 on p is calculated as (Cameron & Trivedi, 2010)

$$\text{Marginal Effects}(X_1) = \beta_1 \times p \times (1-p). \tag{A.2}$$